Katya Dimitrova-Petrova (Orcid ID: 0000-0001-5119-7753)

Rafael Rosolem (Orcid ID: 0000-0002-4914-692X)

Chris Soulsby (Orcid ID: 0000-0001-6910-2118)

Mark E. Wilkinson (Orcid ID: 0000-0001-5169-758X)

Allan Lilly (Orcid ID: 0000-0002-0142-9269)

Josie Geris (Orcid ID: 0000-0003-0159-0543)

Title page

I. Key words

Cosmic ray neutron sensor; soil moisture; spatial variability; portable CRNS; organic-rich soils; managed landscapes; semi-distributed rainfall-runoff modelling

II. Title

Combining static and portable Cosmic Ray Neutron Sensor data to assess catchment scale heterogeneity in soil water storage and their integrated role in catchment runoff response

III. The full name of the authors

Dimitrova-Petrova, Katya [1,2]; Rosolem, Rafael [3,4]; Soulsby, Chris [1]; Wilkinson, Mark E. [2]; Lilly, Allan [2]; Geris, Josie [1]

IV. The authors' institutional affiliations

[1] Northern Rivers Institute, School of Geosciences, University of Aberdeen, Aberdeen, United Kingdom; [2] The James Hutton Institute, Craigiebuckler, Aberdeen, United

Kingdom; [3] Department of Civil Engineering, University of Bristol, Bristol, United Kingdom; [4] Cabot Institute, University of Bristol, Bristol, United Kingdom

V. Corresponding Author's name and contact details

Josie Geris j.geris@abdn.ac.uk

Combining static and portable Cosmic Ray Neutron Sensor data to assess catchment scale heterogeneity in soil water storage and their integrated role in catchment runoff response

Dimitrova-Petrova, Katya [1,2]; Rosolem, Rafael [3,4]; Soulsby, Chris [1]; Wilkinson, Mark E. [2]; Lilly, Allan [2]; Geris, Josie [1]

[1] Northern Rivers Institute, School of Geosciences, University of Aberdeen, Aberdeen, United Kingdom; [2]The James Hutton Institute, Craigiebuckler, Aberdeen, United Kingdom; [3]Department of Civil Engineering, University of Bristol, Bristol, United Kingdom; [4]Cabot Institute, University of Bristol, Bristol, United Kingdom

Abstract

Soil water content (SWC) is a key variable in many land surface processes, such as runoff generation, thus knowledge about its spatiotemporal dynamics at the catchment scale can be useful for constraining and evaluating hydrological models. Cosmic ray neutron sensor (CRNS) technology provides hectare scale SWC data, and with recent advances in mobile CRNS such information value can be extended to the catchment scale, although challenges in calibration remain, especially in wet environments. This study presents a new methodology suited for humid environments to explore spatio-temporal variability in near-surface soil water storage (S_{NS}) dynamics at the catchment scale and its value in semi-distributed rainfall-runoff modelling calibration. For a humid mixed-agricultural catchment (~10km^2) in Scotland, we combined ~4-years of SWC data from a static CRNS at a landscape-representative location with “snapshots” at four key soil-land use (SLU) units to produce SWC timeseries for each one of those units. The SLU units involved a mixture of

freely draining mineral and poorly draining organic-rich soils, supporting crop and livestock farming and moorland, respectively. We also explored the suitability of the standard CRNS calibration approach in the SLU units and found that the organic-rich soils required an adapted parameter calibration for SWC. The moorland SLU unit had the greatest difference in SWC dynamics from the other agricultural SLU units. To explore the additional information generated by the combined CRNS approach, we calibrated a semi-distributed rainfall-runoff model (HBV-light) by using S_{NS} dynamics in individual SLU units in addition to streamflow. Compared to a lumped approach, the semi-distributed SWC information and model structure helped produce better constrained stream flows and further improved the representation of catchment internal storage dynamics. Ultimately, the value of the SWC time series for different SLU units in rainfall-runoff modelling will depend on model structure and the degree to which S_{NS} dynamics vary within the landscape. This study showed the potential of expanding the information value of permanently installed CRNS sensors using portable CRNS surveys while addressing the various challenges related to organic-rich soils and wetter environments, although testing in different environments would be required to evaluate the wider applicability.

Key words:

Cosmic ray neutron sensor; soil moisture; spatial variability; portable CRNS; organic-rich soils; managed landscapes; semi-distributed rainfall-runoff modelling

1. Introduction

Near-surface soil water storage has a key role in regulating evapotranspiration, infiltration, water retention, drainage and hence catchment runoff generation (Brocca et al., 2010; Lilly et al., 2012; Ochsner et al., 2019; Rinderer & Seibert, 2012; Tetzlaff et al., 2007). Due to its importance in many land surface processes, it is a key variable in hydrology, meteorology and agriculture (Vanderlinden et al., 2012; Vereecken et al., 2014; Western et al., 2004), and

crucial for improving land surface modelling *e.g.* to aid model validation and reduce the bias in prediction of water and energy fluxes (Marsh et al., 2020; McJannet et al., 2017). As such, near-surface soil water storage (S_{NS}), or soil water content (SWC, see Appendix I for all abbreviations) in the upper portions of the soil, is estimated by an increasing number of satellite and other observational approaches (Mccabe et al., 2017).

Cosmic ray neutron sensor (CRNS) technology can now provide field average (up to ~7 ha, Schrön et al., 2017) estimates of SWC dynamics at an intermediate scale, addressing difficulties of point scale heterogeneity and the relatively coarse spatial resolution of satellite-derived products (Fersch et al., 2018; Montzka et al., 2017; Sigouin et al., 2016). National-level networks are increasingly being installed to explore variations between sites, e.g. in USA (Zreda *et al.*, 2012), Australia (Hawdon *et al.*, 2014), India (Montzka et al., 2017) and the UK (Cooper et al., 2020) . CRNS data have been used for a wide range of applications, including estimation of hydraulic properties (Brunetti et al., 2019; Foolad et al., 2017; Rivera Villarreyes et al., 2014), validating satellite SWC estimates (Duygu & Akyürek, 2019; Kędzior & Zawadzki, 2016; Montzka et al., 2017) and improving land surface (Baatz et al., 2017; Iwema et al., 2017) and catchment-scale environmental modelling (Dimitrova-Petrova *et al.*, 2020a).

While CRNS probes are customarily employed at a static location providing time series of near-surface soil water contents (SWC) (Bogena et al., 2018; Coopersmith et al., 2014; Nguyen et al., 2017; Schreiner-McGraw et al., 2016), mobile CRNS technology, which includes both rover and portable CRNS applications, has the potential to expand their information value. Despite its relatively large spatial coverage, static CRNS probes are unlikely to capture fully the spatial heterogeneity in near-surface SWC of catchment (>1km^2) or larger scales, where higher level decision making on water resource management is generally made. In recent studies, this has been partially addressed by employing rover CRNS technology, i.e. a CRNS sensor mounted on a vehicle, providing “snapshot” maps of

spatially variable SWC across fields or within catchments. For the small catchment scale (~10 km^2), spatial variability of SWC can be more easily assessed using a portable, i.e. suitcase or backpack version of the CRNS technology (Franz, 2018). Rover CRNS applications include improvement and validation of remote sensing soil moisture products at the regional scale (Chrisman & Zreda, 2013; Dong et al., 2014; McJannet et al., 2017), monitoring and soil mapping of irrigated agriculture (Finkenbiner et al., 2019; Franz et al., 2015; Gibson & Franz, 2018) and SWC characterisation in landscapes with spatially varying land uses (Vather et al., 2019). However, while the rover CRNS approach in these studies provided relatively large spatial coverage and high resolution, it lacked high temporal resolution. Alternatively, dense networks of static CRNS have been installed temporarily to investigate SWC spatiotemporal heterogeneity (Fersch et al., 2020), yet such dense monitoring systems are expensive to establish and maintain in the long term.

Therefore, an experimental framework which combines static CRNS and portable CRNS approaches has the potential to generate valuable SWC information at both relevant spatial- and temporal resolutions (Fersch, 2020; Franz et al., 2015; McJannet et al., 2017). Such an approach could be supported by the fact that at many locations under the same climatic forcing, soil moisture among sites tend to display similar dynamics at daily timescales, although with differences in magnitude. These similarities have been observed at many sites despite marked differences in land use (Choi et al., 2007; Zucco et al., 2014), hillslope position (Penna *et al.*, 2013) or between measurements obtained at different spatial scale but at an overlapping location (Zhou et al., 2007) and soil properties (Gwak & Kim, 2017; Shi et al., 2015). However, studies that have combined static and mobile (in this case rover) CRNS approaches are limited and have mainly been tested in dry climates over large (>100 km^2) areas (Franz *et al.*, (2015) and McJannet *et al.*, (2017)) with only a few examples in temperate sites (Jakobi et al., 2020; Schrön et al., 2018) and none in humid climates.

One challenge is the CRNS sensor calibration requirements for spatially different conditions (e.g. in soil properties or land cover). While the typical calibration of CRNS sensors works well for many sites and soil types (Bogena et al., 2013; Desilets et al., 2010), an additional evaluation of the signal correction or the sensor calibration method might be needed to address certain site-specific conditions (Heidbuchel et al., 2016; Iwema et al., 2015; Rivera Villarreyes et al., 2011). This may be in environments where high organic matter content (e.g. soil organic carbon or plant biomass) dynamically influences the signal (Bogena et al., 2013; Jakobi et al., 2018).

Indeed, in humid environments, where peaty (organic-rich) soils are often present, obtaining accurate SWC estimates remains a challenge (Boorman et al., 2018), due to the distinct water retention characteristics of these soils (Boelter, 1968). Therefore, to successfully apply combined CRNS approaches in wetter regions, testing whether an additional or flexible site-specific calibration of the neutron to soil water content (N-SWC) relationship might be a necessary pre-requisite for creating spatially variable timeseries of S_{NS}.

In northern, humid, mixed-agricultural catchments, near-surface SWC is a key control on runoff generation and runoff threshold response (Brauer et al., 2013; Geris et al., 2015; Seibert et al., 2011). In the UK, soil saturation and flood events are frequent so that accurate and spatially representative SWC data obtained from CRNS data could particularly help improve flood predictions (Bell et al., 2009; Hannaford, 2015; Hundecha et al., 2020). Such landscapes typically involve a patchwork of relatively small fields with variations in soil and land use/management and some proportion of wet, poorly draining moorlands on organic-rich soils (House et al., 2010). Moorlands commonly cover the headwaters of UK catchments and are known to generate large proportions of the runoff that contributes to flooding events (O'Connell et al., 2004). Thus the combination of a representative static CRNS data (Dimitrova-Petrova et al., 2020a) complemented with portable surveys within distinct soil-land use (SLU) units including more moorlands, could provide an integrated approach to

obtain spatially relevant S_{NS} data in typical UK and managed landscapes. The usefulness of such spatially variable S_{NS} information in hydrological modelling should be explored in each context to understand if it carries an additional value as compared to S_{NS} data from a static CRNS location. In addition to hydrological modelling (Percy et al., 2020), there are many other applications which would benefit from having such spatially variable (i.e. across fields or between sub-catchments), high temporal resolution timeseries data, such as improving the efficiency of irrigation schemes (Guo et al., 2020) or evaluating the impact of land management on soil loss (Hallett et al., 2016; Vaezi et al., 2017).

The main aim of this study was therefore to use a combination of static CRNS data and portable CRNS surveys complemented with field-based SWC measurements to explore the spatio-temporal variability in near-surface soil water storage S_{NS} dynamics at the catchment scale in a semi-distributed rainfall-runoff modelling framework. We applied this to a humid mixed-agricultural catchment with a range of soil-land use units including mineral and organic soils typical for the UK. More specifically, the objectives were to (i) explore the relationship between neutron intensities sensed within a landscape-representative footprint using static CRNS and those within individual/contrasting soil-land use (SLU) units using portable CRNS; (ii) based on those relationships, develop a methodology to create synthetic timeseries of daily near-surface SWC for individual SLU units addressing the challenges related to wet organic-rich soils and (iii) derive timeseries of S_{NS} for the individual SLU units and demonstrate their value in semi-distributed catchment scale rainfall-runoff model calibration.

2. Methods

2.1. Site description and instrumentation

The study was conducted in the Elsick catchment (~10 km^2), NE Scotland, UK (Figure 1). Mean annual precipitation is ~800 mm and potential evapotranspiration ~350 mm (Met Office, 2019a, 2019b). The underlying geology is metamorphic bedrock, overlain by glacial drift, covered by relatively thin (0-1m) soils (British Geological Survey, 2019; Soil Survey of Scotland Staff, 1981). The stream network drains a gently sloping landscape (90 to 165 m.a.s.l.) mainly covered by a patchwork of pastoral and arable farms. In this predominantly agricultural landscape, soil properties and land use are linked, forming characteristic soil-land use (SLU) units. In Elsick there are four SLU units that cover ~94% of the catchment and which are characterised by their soil drainage type (Soil Survey of Scotland Staff, 1981) and dominant land use (Table 1., Figure 1). These SLU units are: (i) Crop-Imperfectly drained (CropI), (ii) Crop-Poorly drained (CropP), (iii) Pastures-Freely drained (PastureF) and (iv) Moorland-Poorly drained (MoorlandP). Historically, the poorly and imperfectly drained SLU units associated with agriculture have been artificially drained to enhance crop growth (Blann *et al.*, 2009; Lilly *et al.*, 2012). The less managed, poorly drained MoorlandP sites are located in the catchment's NE headwaters and characterised by an organic-rich surface layer (>40 cm thick). The absence of agriculture and artificial drainage makes surface ponding most frequent in this unit. A minor proportion of the catchment (~6%) has forest plantations on various mineral soils and very minor urban cover (Figure 1).

A static Cosmic neutron ray sensor $CRNS_{static}$ (CRNS −1000/B, Hydroinnova, New Mexico, USA) was used to obtain continuous estimates of near-surface average SWC (SWC_{static}). The $CRNS_{static}$ station (Fig. 1C) was installed in November 2015 at the intersection of three fields (latitude 57°02′25.58″N and longitude 2°11′18.84″W, elevation = 95 m.a.s.l.), which are representative of two of the key SLU in the catchment (Table 1): CropP (Figure 1 E) and PastureF (Fig. 1 D). The $CRNS_{static}$ sensor was calibrated over five field sampling campaigns covering a range of wetness conditions (for full details on the sensor calibration refer to

Dimitrova-Petrova et al., 2020a). The $CRNS_{static}$ continuously records neutron intensity (N_{raw}), temperature (T), relative humidity (RH) and atmospheric pressure (P_{atm}) and, since April 2017, has been complemented by an automatic weather station (Environmental Measurements Ltd.), which measures net radiation (Kipp and Zonen NR Lite2 Net Radiometer), wind speed and direction (WSD1, Environmental Measurements Ltd.) (every 30 minutes), used alongside RH, T and P_{atm} for potential evapotranspiration estimates using the Penman-Monteith method. Precipitation was measured at the $CRNS_{static}$ location using a tipping bucket rain gauge (EML, ARG100 gauge). Stream discharge at the Elsick catchment outlet (Q_{OUT}, in mm day^{-1}) was calculated as the sum of observations at the MAIN and TRIB sub-catchments (Figure 1 A). Gauging across the range of observed levels was used to obtain continuous stream discharge from the stream level data (TD Diver, Van Essen Instruments). Daily precipitation data prior to monitoring (January 2011 – January 2015), were obtained from distance-weighted interpolation using 14 neighbouring gauges from a national monitoring network (Met Office, 2019a) within a 35 km radius of the catchment. This was also used to fill occasional data gaps in precipitation, while site-corrected meteorological data from Dyce Aberdeen Airport (<25km to the north) were used to fill gaps in PET estimates (Met Office, 2019b).

2.2. Portable CRNS data collection and cross-calibration of the CRNS sensors

We combined data from the $CRNS_{static}$ and a portable version ($CRNS_{portable}$) to assess the SWC in the four key SLU units situated outside (Figure 1 A) or within (Figure 1 B) the $CRNS_{static}$ footprint. The $CRNS_{portable}$ is similar to the backpack format described by Franz (2018). It is relatively lightweight and makes spatial surveying time and cost effective, which is well-suited for the heterogeneous landscapes with relatively small fields (Franz, 2018). These portable CRNS sensors, in contrast to the rovers, are less powerful than the static

sensors (~60% in this case), so that a cross-calibration between the two devices is required. Here, the $CRNS_{portable}$ sensor was cross-calibrated with the $CRNS_{static}$ sensor by deploying the $CRNS_{portable}$ for ~8 hours next to the $CRNS_{static}$ (Figure 1 C) on five occasions spanning a range of soil moisture conditions. The neutron counts of each sensor were integrated to 1-hour values (N_{raw} in cph). Following standard procedures, three correction factors were applied (Equation 1 and Equation 2) to account for the influence of atmospheric pressure (fp), incoming solar radiation (fi) and relative humidity (fh) (Evans et al., 2016; Zreda et al., 2012) using the data of P_{atm} (in mbar), RH, (in %) and T, (^{o}C) recorded by each of the CRNS sensors and using a common solar intensity factor, fi (from the Jungfraujoch monitoring station, Switzerland, provided by Hydroinnova via http://nearfld.com). The signal of the $CRNS_{static}$ was additionally corrected for the influence of aboveground biomass using a daily fveg factor (following Baatz et al., (2015)) to produce daily time series of $Npihv_{static}$.

$$Npihv_{static}[cph] = Nraw_{static} * fp_{static} * fi * fh_{static} * fveg_{static} \quad \text{(Eq. 1)}$$

$$Npih_{portable}[cph] = Nraw_{portable} * fp_{portable} * fi * fh_{portable} \quad \text{(Eq. 2)}$$

To account for the poorer potency of $CRNS_{portable}$, the ratio (mean ± stdev) of $Npih_{portable}/Npihv_{static}$ was calculated for different integration times, where we found the ratio to be stable from >4 hours. This ratio at a 4-hour integration time was then used to upscale $Npih_{portable}$ measured at other locations (i.e. within the individual SLU units) to $Ns_{portable}$ (Equation 3) to enable comparable calculations:

$$Ns_{portable}[cp4h] = \frac{Npih_{portable}}{ratio} \quad \text{(Eq. 3)}$$

Next, the $CRNS_{portable}$ sensor was deployed for 8 hrs at each SLU unit (Figure 1) on 3-5 different days, covering a range of wetness conditions. We found that a linear relationship described the correlation between $Npihv_{static}$ and $N_{s\_portable}$ for each SLU unit, as found in other studies in soil moisture spatial heterogeneity (e.g. Lv et al., 2016, Zucco et al., 2014).

The strength of these relationships (as R^2 for linear regression) was tested at integration times from 1 to 8 hours. As R^2>0.5 for the four SLU units was reached again at a 4-hour integration time, we used the regression at 4-hour integration time to derive continuous timeseries of Ns_{SLU} for each SLU unit for the period 13 November 2015 - 31 December 2019 (Equation 4).

$$Ns_{SLU}(t) = a * Npihv_{static}(t) + b \quad \text{(Eq. 4)}$$

Note that no vegetation correction was applied at the individual SLU units as long-term aboveground estimates were lacking for the CropI and MoorlandP units. To test the potential implications of this, we explored the differences between the relationships (Equation 4) using either vegetation corrected and non-corrected $CRNS_{portable}$ data for the CropP and PastureF using t-tests. As no significant differences were found, we used time series of $Npihv_{static}$ and $Ns_{portable}$ to derive the synthetic time series for each SLU unit.

2.3. Synthetic soil water content timeseries for each SLU unit (SWC_{SLU})

To obtain synthetic timeseries of SWC from Ns_{SLU} data for each SLU units (*i.e.* objective (ii)), we complemented the $CRNS_{portable}$ surveys with independent field measurements of SWC on the same days. These were spatially distributed point SWC (θ probe) measurements and topsoil core samples (0-5 cm). For point measurements, we used a ML2 soil moisture sensor (Delta T Devices Ltd) θ probe, integrating over 0-6 cm with an approximate control volume of 30 cm^3. We focussed on the topsoil only as it exhibits most dynamic SWC behaviour and has been shown to strongly influence runoff generation in many agricultural sites in the UK (Gruszowski et al., 2003; Meyles et al., 2003; Withers et al., 2007). On average 140 SWC measurements in each SLU unit, on each sampling day, were made along four, 0-70 m transects radiating from the $CRNS_{portable}$ location, at 90° to each other. Occasionally, technical difficulties or frozen ground limited the number of measurements possible. Usually, a minimum of two replicates were taken every 2 meters

from 0 to 25 m distance, every 5 meters from 25 to 40 m and every 10m from 40 to 70m. The measurements taken with the θ probe on each sampling day (θ_{SLU}) were weighted following Schrön et al., (2017) to obtain the average soil moisture estimate for each SLU on each day.

The 0-5cm depth soil cores were used to determine mean dry bulk density (ρ_{dry}, in [g cm^{-3}]), soil organic matter (SOM, in [cm^3 cm^{-3}]) and lattice water (LW, i.e. the water contained in soil minerals, in [cm^3 cm^{-3}]) for each SLU unit. The ρ_{dry} was determined by oven-drying each sample (24h/105^{o}C) and correcting for stones (Hall et al., 1977), and SOM and LW estimated by loss-on-ignition (firstly 24h/450^{o}C for SOM and then 6h/1000^{o}C, for LW) (Davies, 1974).

The ρ_{dry}, SOM and LW for the CropP and PastureF units within the static footprint were characterised from the 0-5 cm samples from five campaigns also used to calibrate the static CRNS (Dimitrova-Petrova et al., 2020a) (n=48 for CropP and n=26 for PastureF, respectively). The ρ_{dry}, SOM and LW of the SLU units outside the footprint, *i.e.* CropI and MoorlandP, were characterised from a single soil sampling campaign (n=9 for the CropI and n=6 for the MoorlandP, respectively). While the sampling size for these estimates is relatively small, this is justified by the relatively low spatial variability revealed from the ~140 topsoil point SWC measurements on each sampling day in each SLU unit, and again by relatively low vertical variability for the agricultural fields as revealed by (Dimitrova-Petrova et al., 2020a).

To determine the wetness conditions under which $CRNS_{portable}$ sampling took place in contrasting SLU units, we explored different proxies for catchment wetness alongside topsoil point-scale SWC (θ_{SLU} and soil cores). These proxies included stream discharge at the catchment outlet (Q_{OUT}, in [mm day^{-1}]), the 7-day antecedent precipitation index (API_7, in [mm]) using daily precipitation data with a constant decay coefficient of 0.9 (Hooke, 1979), and the landscape-average soil water content estimated by the $CRNS_{static}$ (SWC_{static} in [m^3 m^{-

306 ^{3}]). The latter also allowed for a more direct evaluation of the relative differences between
307 SLU units and the $CRNS_{static}$ footprint. There were differences in soil properties between the
308 static and portable sites, particularly in soil organic content, which was substantially greater
309 at the MoorlandP unit. The procedure to account for those differences included a
310 transformation of the $CRNS_{static}$ time series into synthetic time series of SWC for individual
311 SLU units (SWC_{SLU}) and testing the need for additional calibration of the shape parameters
312 (a_i) alongside N_0 in Equation 5, which represents the function used to transform neutron
313 counts to SWC data.

314 $$SWC_{SLU}(t) = \left(\left(\frac{a_0}{Ns_{SLU}(t)/N_0 - a_1} \right) - a_2 \right) * \rho_{dry} - (LW + SOM) \quad \text{(Eq. 5)}$$

315 for which SWC_{SLU} is in [m^3 m^{-3}], Ns_{SLU} is in [cph], N_0 is the theoretical site-specific value of
316 count rate over dry soil in [cph] (Desilets et al., 2010), and a_i are shape coefficients. The ρ_{dry}
317 [g cm^{-3}], LW [m^3 m^{-3}] and SOM [m^3 m^{-3}] are the estimated dry bulk density, lattice water and
318 soil organic matter, respectively, as described above. The SWC_{SLU} time series were
319 additionally constrained. Total porosity was used as an upper limit, which meant that for
320 SWC values above it, we assumed that the soils were saturated and any additional reduction
321 in neutron counts was related to surface water ponding. Total porosity was estimated to be
322 0.6 for the managed SLU units and 0.8 for the MoorlandP. Lower SWC limit for the mineral
323 SLU units was set to the minimum measured value at each unit (0.10 m^3 m^{-3} in the CropP
324 and 0.13 m^3 m^{-3} in the PastureF, see Dimitrova-Petrova *et al.*, 2020b; 0.07 m^3 m^{-3} at the
325 CropI), while for the MoorlandP the lower SWC limit was set to 0.55 m^3 m^{-3}, based on field
326 knowledge on soil water retention and previous research on peaty podzols in Scotland
327 (Tetzlaff et al., 2014).

328 In most CRNS applications, typically only N_0 in Equation 5 is optimised, while all soil
329 properties are determined from field observations (e.g. Evans *et al.*, 2016; McJannet *et al.*,

2017). The shape coefficients of the equation are normally fixed at reference values of a_0=0.0808 [$cm^3\ g^{-1}$], a_1=0.372 [-] and a_2=0.115[$cm^3\ g^{-1}$]), derived by (Desilets et al., 2010) via neutron flux simulations for generic silica soils. However, some have identified the need for additionally calibrating the a_i parameters to reproduce site-specific SWC dynamics or match local conditions (e.g. Iwema et al., 2015; Rasche et al., 2021; Rivera Villarreyes et al., 2011). Here, we tested if such new calibration is needed to better fit field observations and hence allow consideration of site differences between SLU units, particularly in soil hydraulic properties and wetness dynamics, which is especially relevant for the peaty soils at MoorlandP.

For each SLU, we therefore tested two sensor calibration approaches based on the SWC data from the SLU to derive SWC_{SLU} from Ns_{SLU}, while using the site specific ρ_{bulk}, LW, SOM and SWC (θ_{SLU}) data for Equation 5. More specifically, the first approach involved the typical standard N_0 calibration (Bogena et al., 2013), with fixed shape (a_i) parameters and optimization of only the N_0 parameter in Equation 5 (Table 2). In the second approach, referred here as new calibration, we simultaneously calibrated the N_0 and a_i shape parameters. For this we used the Latin Hyper Cube approach (McKay, 1992) (Table 2). We performed 100 000 runs from which we obtained a single best parameter set, minimising the root mean square error (RMSE) and which fitted the field data best (i.e. daily averages of Ns_{SLU} and field θ_{SLU} measurements on sampling days). The optimised parameters for each calibration were then used to solve Equation 5, producing two synthetic SWC timeseries per SLU unit, SWC_{typ} and SWC_{new}, respectively.

To evaluate the new additional calibration of the shape parameters, we considered the potential improvement in fit to the data and the uncertainty around extremely wet or dry SWC estimates associated with the SWC constraints. We also calculated for each SLU unit the root mean square difference (RMSD) between the synthetic SWC timeseries produced with the typical and the new calibration, respectively (Equation 6).

356 $$RMSD = \sqrt{\frac{\sum_{t=1}^{t=n}\left(SWC_{typ,t} - SWC_{new,t}\right)^2}{n}} \quad \text{(Eq. 6)}$$

357 In this equation, the $SWC_{typ,t}$ is mean soil water content estimate at time t, derived from
358 Ns_{SLU} using a SLU-specific N_0 and fixed a_i parameters (Table 2). Correspondingly, $SWC_{new,t}$
359 is the soil water content derived from Equation 5, using the best parameter set of N_0 and a_i
360 from the Latin Hyper Cube simulations. A poor fit to the field data, a high proportion of
361 unrealistic estimates using the standard approach, plus a relatively small RMSD all indicated
362 the need for the additional calibration of the shape parameters to obtain SWC data. After the
363 evaluation, only one time series SWC_{SLU} (i.e. either the typical or new sensor calibration
364 approach) per SLU unit was chosen for further calculations.

365

366 **2.4. Spatially variable CRNS-derived near-surface storage (S_{NS_SLU})**
367 **estimates for rainfall-runoff model calibration**

368 The SWC data were then used to derive time series of near-surface water storage for the
369 individual SLU units (S_{NS_SLU}) and combine them with stream discharge in multi-criteria
370 model calibration of a semi-distributed rainfall-runoff model for the catchment (objective iii).
371 For that we used a semi-distributed version of the HBV-light model (Lindström et al., 1997;
372 Seibert & Vis, 2012), which is a conceptual rainfall-runoff model that simulates discharge
373 Q_{sim} using a minimal input time series of precipitation (P), air temperature (T) and potential
374 evapotranspiration (PET). The hydrological model comprises four main components: a snow
375 (snow accumulation and melt), a soil (groundwater recharge and AET), a response
376 (computes run-off as function of storage) and a routing (triangular weighting function for
377 routing run-off to catchment outlet) routine (Seibert & Vis, 2012).

378 The model was set up for Elsick at daily time steps using P, T and PET input from 1 January
379 2011 to 31 December 2019, allowing for a relatively long warm-up period to eliminate the

effects of initial conditions, especially on storage. Q_{OUT} was available from 12 January 2015 to the end of the study period. While the effect of snow is accounted for, the parameters of the snow routine were fixed and not calibrated (see Supplementary Table 1), as snow contribution to precipitation in the catchment is minor. To simulate the presence of four SLU units in the catchment we opted for a model structure with four distributed soil zone reservoirs (SM) and the upper (SUZ) stores, while the lower model store (SLZ) was lumped. Each of the four SM and SUZ were given a weight corresponding to the proportion of the catchment covered by a specific SLU (Table 1), rescaled from a total of 94% catchment area to add up to 100%. While the SM represents the soil zone dynamics, the SUZ and SLZ roughly represent the shallow and deeper run-off generating stores, respectively. For Elsick, we conceptualised the HBV-light dynamic storage S_{dyn} (t) i.e. the storage activated in the runoff generation response as the sum of SM and SUZ at a given moment in time in each of the four semi-distributed stores. The rationale being that SM is responsible for the partitioning of precipitation input to deeper storage and ET, but does not produce runoff, while SUZ is the upper box that above a certain threshold (UZL parameter) generates Q_{sim}. This combined storage is considered equivalent to the role of the near-surface soil water storage (S_{NS}), which the CRNS senses. On the other hand, the S_{NS_static} or S_{NS_SLU} represent the total water storage for a predetermined physical depth as opposed to S_{dyn}, which, as in most conceptual rainfall-runoff models, is not bound to a specific depth. Therefore, a direct comparison of S_{NS} estimates (S_{NS_static} or S_{NS_SLU}) with modelled storage dynamics S_{dyn} is not straightforward, here we opted for comparing the total soil column storage 0–400mm (S_{NS_SLU}) to S_{dyn}, similar to Dimitrova-Petrova et al. (2020a).

To prepare storage data for the model calibration, we converted time series of SWC_{static} and SWC_{SLU} to S_{NS_SLU} using an exponential filter (as in Dimitrova-Petrova *et al.*, (2020a)) for the period 14 Nov 2015 – 31 December 2019. Next, the semi-distributed HBV-light rainfall-runoff model for the catchment was calibrated using the four S_{NS_SLU} as well as catchment Q_{OUT}.

The model calibration period was 13 November 2015 to 31 December 2019 (~4 years). Days on which S_{NS_SLU} data were missing were not included in the model calibration. We used a Monte Carlo approach (100,000 independently generated parameter sets) for model calibration. Initial parameter ranges were set based on literature values (Seibert & Vis, 2012; Tetzlaff et al., 2015) and exploratory model runs (Supplementary Table 1). To account for model uncertainty, each model run was ranked according to the multiple-criteria (Pareto) ranking of model performance (following Rosolem et al., 2012). For each model run, this involved ranking of five criteria, which were the KGE goodness-of-fit (Kling-Gupta efficiency, Gupta et al., (2009)) of the Q_{OUT} to simulated discharge (KGE_Q_{sim}) and of the time series of S_{NS_SLU} to the corresponding simulated dynamic storage dynamics ($KGE\_S_{dyn\_SLU}$).

Consequently, we calculated the minimal Euclidian distance within the KGE space across the five criteria to select the best 50 parameter sets. As part of this, the five KGE criteria received different weights. A weight of 50% was assigned to the KGE of discharge (i.e._Q_{sim}), and 50% to the internal storage dynamics $KGE\_S_{dyn\_SLU}$, with weight proportional to their rescaled coverage of the SLU unit in the catchment. Equation 7 summarises the final multiple objective criteria ($KGE_{multiple}$) used here:

$KGE_{multiple}=$

$$\sqrt{0.5 * \left(1 - KGE_{Qsim}\right)^2 + \frac{0.18}{0.5} * \left(1 - KGE_{Sdyn\_PastureF}\right)^2 + \frac{0.37}{0.5} * \left(1 - KGE_{Sdyn\_CropI}\right)^2 + \frac{0.34}{0.5} * \left(1 - KGE_{Sdyn\_Cro}\right.}$$

(Eq. 7)

We also evaluated similarities and any differences in optimisations of identifiable parameters.

3. Results

3.1. Hydrometeorological and wetness conditions during study period

Continuous monitoring at Elsick spanned 1505 days (~ 4 years), covering a range of hydrometeorological conditions (Figure 2). The SWC_{CRNS} ranged between 0.14 at its driest and 0.6 at saturation (median was 0.37 m^3 m^{-3}). Observations at the $CRNS_{static}$ started during an exceptionally wet winter in 2015-16, characterised by large precipitation events and floods (Figure 2 A). This was followed by a period of more seasonal wetting-drying cycles (March 2016 – June 2017). August 2017 – April 2018 was relatively wet and included a large rain on snow event in March 2018, which caused local flooding. The $CRNS_{portable}$ surveys started during the summer of 2018, which was characterised by a prolonged streamflow recession and continuous soil drying, to capture the driest conditions observed at the catchment (Figures 2 C and C.1.). In the managed SLU units, average field SWC values, as measured with the theta probe (θ_{SLU} at depths 0-6 cm), were close to or slightly greater than SWC_{static}, while $\theta_{MoorlandP}$ was consistently much wetter. After subsequent rewetting, more surveys were conducted in all the SLU units during December 2018 – April 2019 and December 2019 to capture wetter soil conditions, respectively (Figures 2 C, C.2 and C.3). During these wetter soil conditions, average θ_{SLU} was greater at the CropP, PastureF and especially MoorlandP units as compared to SWC_{static}. During those periods, the field SWC at CropI (θ_{CropI} and soil cores) showed similar values to the SWC_{static} and the MoorlandP was consistently wetter, according to field measurements ($\theta_{Moorland}$ and soil cores). The θ_{SLU} spatial heterogeneity on each sampling day (indicated by standard deviations in Figure 2) was generally small but relatively large during dry and intermediate periods. During wet periods it was generally smaller and similar in all the SLU units, except for CropI, for which was similar across all wetness conditions.

Field sampling of SWC in each SLU unit covered a similarly wide range of wetness conditions, as illustrated by comparing field SWC to three proxies of catchment wetness (Figure 3). Daily SWC_{static} displayed a strong linear relationship to the field SWC data in each

SLU unit (Figure 3 A). The managed SLU units within the static footprint (i.e. CropP and PastureF) were very well characterised, as sampling encompassed the 2nd to the 93rd percentiles of SWC_{static}. The CropI and MoorlandP units outside the $CRNS_{static}$ footprint, were sampled under most wetness conditions, across the 3rd and 60th percentiles. Overall, the range of SWC measured in each managed SLU unit were similar to those in $SWC_{static,}$ while the MoorlandP was distinctly wetter. Field SWC data generally increased with API_7 and Q_{OUT} (Figure 3 B and C, respectively). For variations with Q_{OUT}, threshold behaviour was evident, which is in line with findings on storage – discharge relationships in the catchment, reported in Dimitrova-Petrova *et al.*, (2020a).

3.2. Relationships between static and portable CRNS neutron data across SLU units

The cross-calibration of CRNS probes was carried out over five sampling days (Figure 2 C, C.1. and C.2.). Neutron intensities corrected for atmospheric influences from the two sensors, $Npih_{\_static}$ and $Npih_{\_portable}$, respectively, related linearly (R^2=0.99), as shown in Figure 4 A. The mean ratio of 0.654 between them (Figure 4 B) was used to scale the neutron intensities of the $CRNS_{portable}$ (Equation 3). The sampling covered very dry to intermediate conditions, corresponding to very high (up to 99th percentile of $Npih_{\_static}$) and moderate neutron intensities (down to 40th percentile of $Npih_{\_static}$), respectively (Figure 4 A). The daily average SWC_{static} on those days ranged between 0.17 to 0.37 m^3 m^{-3} (2nd to 50th percentile of SWC_{static}) and the average θ_{static} (hand-held probe) ranged between 0.16 and 0.49 m^3 m^{-3}. Thus the θ probe measurements seemed to overestimate soil moisture as compared to the CRNS SWC_{static} during wet conditions, as it gives measurements at relatively shallower depths compared to the CRNS.

479 The scaled $CRNS_{portable}$ neutron intensity data (Ns_{SLU}) of each individual SLU unit showed a
480 linear relationship (R^2 >0.5) to the $CRNS_{static}$ neutron count data ($Npihv_{static}$), at a 4-hr
481 integration time (Figure 5). The R^2 of that relationship ranged from 0.52 for CropP, and 0.79
482 to 0.98 for the remainder of the units. Consistent with the CRNS approach, the greatest
483 neutron intensities corresponded with the driest sampling conditions (Figure 5, in red), while
484 the least corresponded to wet or frozen soil conditions. There were subtle differences in the
485 relationship of the SLU units within the $CRNS_{static}$ footprint (Figure 5 A, B). At the CropP unit
486 (Figure 5 A), the Ns_{SLU} data were more variable but close to $Npihv_{\_static}$. Such minimal
487 differences relate logically to the fact that CropP unit occupies ~75% of the $CRNS_{static}$
488 footprint. For the PastureP unit (Figure 5 B), representing ~25% of $CRNS_{static}$, there were
489 even fewer notable differences between Ns_{SLU} and Npih_static. The CropI, situated outside
490 the footprint of $CRNS_{static}$, appeared to have generally greater neutron counts as compared
491 to $CRNS_{static}$, which was most pronounced during drier sampling conditions (Figure 5 C). At
492 the wet MoorlandP unit neutron intensities were much lesser than $Npih_{\_static}$ and also than
493 any of the managed SLU units (Figure 5 D). The N_{s_SLU} from the MoorlandP unit also
494 seemed to experience relatively less variability in neutron counts, as evidenced by the
495 smallest slope of the linear relationships in Figure 5.

496

497 **3.3. Synthetic SWC timeseries for different Soil Land Use units**

498 Soil property field data showed that the ρ_{bulk} of the mineral soils (~1 g cm^{-3}) was much
499 greater than for the organic-rich soil (0.28 g cm^{-3}), while SOM was six times less (Table 4).
500 Moreover, the soil properties of all the mineral soil SLU units correspond with those in the
501 $CRNS_{static}$ footprint. N_0 values for all SLU units used for the typical sensor calibration were
502 greater, but all were within +15% of the N_0 for the static; differences being largest for the
503 MoorlandP unit (Table 4).

Comparison between the typical and new calibration (Figure 6, in red and green, respectively) revealed that through the typical calibration, field data fitted reasonably well for the managed SLU units within the $CRNS_{static}$, CropP and PastureF (Figure 6 A and B, respectively). The new calibration was associated with no improvement in data fit and large RMSE, 0.033 and 0.035 m^3 m^{-3}, for the CropP and PastureF, respectively. Both typical and new sensor calibration produced a good fit to the data for the CropI unit, although the improvement in terms of reproducing the range of SWC using the new calibration was minimal (Figure 6 C, Table 4). In the case of the MoorlandP, only the new calibration produced realistic SWC dynamics (Figure 6 D, in green) with a good fit to the data, associated with the smallest RMSE (0.006 m^3 m^{-3}) (Table 4).

To produce the synthetic SWC timeseries, the typical calibration was kept for the managed SLU units, in- and outside the $CRNS_{static}$ footprint, and the additional parameter calibration was used solely for the MoorlandP unit. The timeseries of Ns_{SLU} for each unit showed very a similar range and overall dynamics to the $CRNS_{static}$ in the case of the managed SLUs (Figure 7 A). For the MoorlandP unit, neutron intensities were much lesser and showed less variability. This related to it being consistently wet, with fewer changes in SWC, compared to the managed units (Figure 7 B). Indeed, relative differences in terms of neutron intensity translated in similar patterns in terms of estimates for SWC_{SLU} (Figure 7 B), effective sensing depth (z_{eff}) (Figure 7 C) and S_{NS} (Figure 7 D). In terms of estimated SWC_{SLU}, the managed SLU units displayed a more dynamic behaviour, as compared to SWC_{static}. During dry conditions estimated SWC_{SLU} values were close to the SWC_{static} and much greater during intermediate and wet conditions (Figure 7 B). During the study period z_{eff} of the $CRNS_{static}$ ranged between 7 and 18 cm (mean 11 cm), with z_{eff} for the mineral SLU units again showing very similar mean and ranges. The z_{eff} in the MoorlandP varied very little, being 7±1 cm, which relates to the reduced sensing depth of CRNS sensors when soils are wetter.

3.4. Comparison between near-surface soil water storage estimates (S_{NS}) from individual SLU units and at the catchment-scale (for rainfall-runoff modelling input)

The two SLUs with crops showed very similar dynamics in S_{NS}, while the PastureF was overall wetter than these other two mineral soils, especially during winter (Figure 7 D; Table 5). The MoorlandP generally followed the wetting and drying cycles but was much wetter than all of the mineral soil units and often saturated, consistent with field observations. Compared to the S_{NS_static}, the S_{NS_SLU} of the mineral SLU units showed greater variability (apart from the MoorlandP), and while all of the units were wetter on average, CropP and CropI were drier during dry periods (Table 5).

The outcomes of the multi-criteria calibration of the HBV-light semi-distributed for the Elsick catchment are shown in Figure 8 and their goodness of fit to observed data in Table 3. Overall, the model simulated discharge well across wetness conditions, except for the period April – October 2019, where Q_{sim} was overestimated (Figure 8 A). The overall performance of the model calibrated using multiple criteria relates to the final parameter ranges (Supplementary Table 1). The 50 best parameter sets according to the multiple calibration criteria yielded median $KGE_{multiple}$ of 0.51 and $KGE_{multiple}$ ranged between 0.49 and 0.52. Across the five criteria KGE_Q_{sim} ranged between 0.63 and 0.74 (median 0.70) (Table 3). For these best 50 runs, the S_{dyn} was fairly well constrained for all of the SLU units and corresponded well with the observed storage dynamics (Figure 8 B, C, D, E). However, for S_{dyn_CropP}, calibrated on S_{NS_CropP} data, the model overestimates the S_{NS} during the dry period and then recovery, from April 2018 onwards (Figure 8 D). The uncertainty bands of the different S_{dyn} may additionally be related to the weight assigned to each KGE_S_{dyn} (Equation 7) i.e. narrower uncertainty band is related to a higher proportion of the weight assigned to a SLU unit. For example, S_{dyn_CropI} calibrated using S_{NS_CropI}, which covers 37% of the catchment (Figure 8 C) shows much less uncertainty as compared to $S_{dyn\_PastureF}$, calibrated

556 on the $S_{NS\_PastureF}$, which only covers 18%. For the 50 best runs across the five criteria, the
557 median KGE_S_{dyn} for the three mineral soils SLU units were similar, ranging between 0.33
558 and 0.40 and the median KGE_$S_{dyn_MoorlandP}$, calibrated on the organic-rich soil data was
559 0.31. For comparison, median KGE_S_{dyn} when individual calibration criteria were used (data
560 not shown) varied between 0.43-0.50 for the mineral units and it was 0.38 for the MoorlandP.

561 Overall, final parameter ranges of the four S_{dyn} were comparable, with a few exceptions.
562 Within the soil routine, the LP parameter which controls evaporation from the soil box was on
563 average higher in the $S_{dyn\_MoorlandP}$, which related logically to the MoorlandP having more
564 available storage for evapotranspiration (Supplementary Table 1). Within the response
565 function, the $K0_{MoorlandP}$ and $K1_{MoorlandP}$ parameters, that are related to the outflow rate, were
566 relatively different for the $S_{dyn\_MoorlandP}$ as compared to the S_{dyn} of mineral soil SLUs. The
567 median $K0_{MoorlandP}$ related to the recession rate of quick flow was larger for the $S_{dyn\ MoorlandP}$ as
568 compared to S_{dyn} for the mineral soils, possibly relating to relatively less available soil
569 storage for runoff modulation (Supplementary Table 1). The median $K1_{MoorlandP}$ was relatively
570 lower, as compared to the mineral units, directly relating to the fact that the MoorlandP SLU
571 unit presents naturally poorer drainage in the upper layers.

572

573 # 4. Discussion

574 ## 4.1. Using CRNS technology to explore relationships between soil
575 ## moisture dynamics of different soil-land use types

576 We explored the relationships between neutron intensities sensed within the static CRNS
577 footprint and those within key soil-land use units (objective (i)) using a combination of static
578 and portable CRNS sensors. The methodology we developed strived for an efficient
579 approach to characterise spatio-temporal SWC dynamics across different SLU units from
580 timeseries of static CRNS sensors. The need for a simple yet reliable way to relate soil

moisture datasets collected at different scales or with different spatial coverage is a key issue in hydrology and environmental modelling (Brocca et al., 2012; Pachepsky & Hill, 2017; Peters-Lidard et al., 2001; Peters-Lidard et al., 2017). Here we showed the potential of combining static and portable CRNS sensors to characterise distinct SLU units within a small (~10 km^2) catchment. We made use of landscape representative neutron count and SWC timeseries from a static CRNS (Dimitrova-Petrova *et al.*, 2020a) and related these to neutron measurements at key soil-land use units within the catchment, using a portable CRNS. This was combined with SLU-specific SWC and soil hydraulic properties information collected in the topsoil (0-6 cm).

Given that a representative location can be identified, many (data-intense) studies have found that under the same climate, point-scale time series of SWC at neighbouring sites can correlate well, despite contrasting soil, land use or topography (Lv et al., 2016; Mittelbach & Seneviratne, 2012; Zucco et al., 2014). Therefore, due to this commonly observed soil moisture temporal stability (Vachaud et al., 1985), it could be possible to use simple (linear) relationships to relate SWC dynamics at different locations and depths (Rosenbaum et al., 2012; Zhao et al., 2020), rescale SWC data, or use datasets from nearby locations for modelling purposes (Peterson et al., 2016; Seibert et al., 2011; Verrot & Destouni, 2016). This is on the condition that the spatial patterns and relationships between sites are known. There are also limitations with regards to the empirically derived linear relationships as these are unlikely to account for all localised short-term changes in SWC at individual SLU units. Nevertheless, applying these concepts to larger (field) scale patterns showed that such spatio-temporal information on near-surface soil water content can be obtained using CRNS technology. Ideally, this would be supported by a dense network of static CRNS sensors (as e.g. in Heistermann et al. 2021), although for most applications this would be unrealistic in terms of available resources. Our approach could therefore be proposed as a trade-off between the number of sensors and the requirements for continuous SWC estimates for key

607 soil-land use units within the catchment. Considering that new cheaper detectors are
608 becoming available on the market (e.g. Stevanato et al., 2019), we believe that our approach
609 can be applied at locations where static CRNS are permanently installed and could extend to
610 nearby ungauged catchments.

611 We demonstrated that the combined CRNS approach is well-suited to patchwork, mixed-
612 agricultural landscapes which are characterised by spatially distributed farm fields with
613 varying soil and land use properties (Hallett et al., 2016). In such context, installing and
614 maintaining point-scale sensors is challenging due to soil management (e.g. harvesting,
615 ploughing) as well as financial and access constraints (Vather *et al.*, 2019; Dimitrova-
616 Petrova *et al.*, 2020a). The limited road network and generally wet soils make the use of a
617 rover CRNS, impracticable. Such challenges can be tackled, as in the present study, by
618 identifying key SLU units and complementing the static with a portable or “backpack” CRNS
619 to assess spatial variability of near-surface soil water storage.

620 This initial assessment of the applicability of the combined CRNS approach was helpful both
621 to address issues specific to the environment (wet climate and organic-rich soils, see section
622 4.2.), but also to identify future improvements. In this study, conversions from neutron count
623 data to the synthetic SWC_{SLU} timeseries at the SLU units were supported by comprehensive
624 ground truthing with a theta probe as well as soil sampling covering the CRNS footprints.

625 We found that the SWC spatial heterogeneity revealed by the theta probe SWC data within
626 each SLU unit on each sampling day was relatively small. Nevertheless, soil agricultural
627 management may introduce variations of soil hydraulic properties and hence soil moisture
628 along the soil profile which may not be deducible from the SWC measured at the topsoil
629 (Hupet & Vanclooster, 2002a; Wallace & Chappell, 2020). At the study site, this was only
630 moderately evidenced. Soil sampling within the footprint revealed little variation in SWC with
631 depth up to 30 cm during five calibration campaigns comprising a range of
632 hydroclimatological conditions. A 30 min record of profile point-scale SWC measurements

633 next to the $CRNS_{static}$ (Dimitrova-Petrova et al., 2020a) also revealed that. For most of the
634 time, especially in wet periods, the topsoil showed similar SWC dynamics and magnitude to
635 lower depths (20 and 30 cm), although it was drier in intermediate and dry periods. In
636 addition to the fact that the impact on neutron signal strongly decreases with depth (Schrön
637 et al.2017), we therefore limited our measurements in the other units to the top 5 cm of the
638 soil. Nevertheless, especially during drier conditions (Figure 7 C) and at drier sites (Franz et
639 al., 2012), the effective sensing depth of the CRNS technology can extend to 30 cm, which
640 should be considered in similar future studies. Additionally, the combination of theta probe
641 measurements with SWC information soil samples may not always lead to better
642 characterised relationships between SLU units (see Figure 3 A, where larger spead in SWC
643 data yields to lower R^2 for two of the SLU units). Indeed, to better characterise the managed
644 SLU units using fewer points but with measurements of soil moisture deeper within the soil
645 profiles would help to improve the portable CRNS signal SWC estimates and reduce
646 uncertainty Baroni *et al.*, (2018), while still sufficiently accounting for spatial heterogeneity.

647 Overall, more sampling would be recommended. Although the appropriateness of the linear
648 transformation was demonstrated by McJannet et al., (2017) in semi-arid Australian
649 landscape, sampling at intermediate wetness would then also allow to further evaluate and
650 refine the linear relationship between static and portable CRNS neutron counts in Elsick (as
651 shown in Figure 5). Most importantly, additional SWC information during intermediate
652 wetness conditions would help to better define the curve of the N-SWC relationship (as
653 shown in Figure 6). If these relationships could be characterised with more certainty, the
654 approach could then be applied in future sampling campaigns without more reliance on the
655 labour-intensive point scale measurements for sensor calibration.

656 Nevertheless, despite these uncertainties, using the combined CRNS approach we were
657 able to characterise SWC dynamics at all key SLU units in the Elsick catchment, including
658 the distinctly wetter MoorlandP SLU unit, which is generally more challenging to monitor

659 (Bartalis et al., 2007; Tetzlaff et al., 2014). Differences between cropped sites (CropP and
660 CropI) were found to be very small, likely due to the similar soil management they are
661 subjected to (i.e. ploughing and presence of artificial soil drainage) (Boland-Brien et al.,
662 2014; Hupet & Vanclooster, 2002). The PastureF was found to be the wettest managed SLU
663 unit, with frequent surface ponding. Even though these soils are naturally freely draining,
664 cattle grazing is thought to have caused compaction and thus greater water retention at the
665 soil near-surface (Meyles e al., 2001; Wallace & Chappell, 2020). Similar conclusions were
666 drawn at the study site using soil water isotope sampling and transit time modelling
667 approaches (Dimitrova-Petrova *et al.*, 2020b).

668

669 **4.2. CRNS applications in humid environments**

670 When creating synthetic time series of daily SWC for each SLU unit, our combined CRNS
671 approach needed to account for site specific challenges i.e. the wet climate and presence of
672 often saturated organic-rich soils (objective (ii)). The CRNS measurements have greater
673 statistical uncertainty at lower neutron count rate, decreasing with longer integration time.
674 This is specifically an issue in humid (Evans et al., 2016) and low-lying (Hawdon et al., 2014)
675 catchments such as Elsick. To account for the uncertainty related to lower count rate, we
676 deployed the portable CRNS at a single location representative for a SLU unit for 8 hours.
677 This appeared as the only feasible option in this landscape, as opposed to using a rover
678 CRNS. The generally more dynamic near-surface water storage estimates at the individual
679 units (S_{NS_SLU}), as compared to the S_{NS_static} are likely to be related to the inherently higher
680 uncertainty in the wetter range of the N-SWC relationship and could also have been the
681 result of SWC_{SLU} overestimations during wet periods. On the other hand, the static CRNS
682 was positioned at a location to provide integrated dynamics across several SLU units,
683 therefore reflecting a more damped signal. This is reflected in the slope of the linear
684 relationship between neutron counts of static and portable CRNS (Figure 5).

685 The presence of often saturated organic-rich (peaty) soils at Elsick, and many similar UK
686 catchments (Lilly et al., 2015), posed additional challenges to the CRNS application. We
687 identified that the moorland soils had distinct hydraulic properties, i.e. lesser bulk density,
688 greater soil organic matter content and greater porosity (Bruneau & Johnson, 2014; Meyles
689 et al., 2001; Tetzlaff et al., 2014), compared to the mineral soils. For sites with greater
690 organic matter content, it has been shown that applying CRNS technology can indeed be
691 challenging (Bogena et al. , 2013; Fersch et al., 2018; Heidbuchel et al., 2016) and
692 accounting for the effect of high organic matter on the CRNS signal often requires additional
693 sampling effort (Jakobi et al., 2018; Vather et al., 2020). In organic-rich, near-saturated soils,
694 using the reference (typical) Neutron Count-SWC (N-SWC) equation can lead to
695 unrealistically dynamic SWC estimates. However, we showed that adequate characterisation
696 could be easily achieved by additionally calibrating the shape (a_i) parameters determining
697 the shape of the N -SWC relationship. We proposed the use of a simple and relatively easy
698 to implement Latin Hypercube approach. This is consistent with findings for other CRNS
699 applications which demonstrated the need of the additional a_i parameter calibration
700 (Heidbuchel et al., 2016; Iwema et al., 2015; Rivera Villarreyes et al., 2011), although the
701 needs for this should be evaluated locally (Iwema et al., 2015). While we sought the need to
702 additionally calibrate the a_i parameter given the distinct soil hydraulic characteristics of the
703 organic-rich soils, we do recognise that perhaps a more comprehensive soil sample dataset
704 could reduce the uncertainty in the N-SWC for this SLU unit more.

705 While it might require the new sensor calibration, CRNS still has an advantage over point-
706 scale measuring techniques in providing more spatially representative SWC estimates,
707 overcoming spatial heterogeneity issues (Brunetti et al., 2019). Moreover, unlike other
708 approaches (e.g. time domain reflectometry or TDR), the measurements are unaffected by
709 temperature (Rivera Villarreyes et al., 2011) and due to the sensor design, lesser likely to be
710 affected by saturation (overland flow, ponding).

711 Robust characterisation of SWC dynamics in humid landscapes has implications for flood
712 and agricultural management. In particular, organic-rich peaty soils, which usually occupy
713 the headwaters of many northern catchments (House et al., 2010), are both key to better
714 understanding their distinct hydrological functioning (Boorman et al., 1995) and challenging
715 to characterise with conventional techniques. In this study, the inclusion of the overall wetter
716 MoorlandP SWC in the $S_{NS\_portable}$ estimates was logically related to the generally wetter areal
717 average of SLU $S_{NS\_portable}$, as compared to those observed with the static CRNS estimates
718 alone. Additionally, the presence of moorlands on peaty soils in agricultural land bears
719 multiple potential management benefits for farmers and policy makers including improved
720 water quality and reducing the risk of erosion and flash flooding (Brown, 2020; Mcbride et
721 al., 2017; RSPB, 2020). Thus, improved knowledge of their near-surface storage dynamics
722 would be useful for management strategies, including flood warning applications.

723

724 **4.3. How and when can spatially distributed information on near-surface**
725 **soil water storage (S_{NS}) help to calibrate rainfall-runoff models?**

726 We derived time series of near-surface soil water storage CRNS (S_{NS}) estimates for
727 individual SLU units and demonstrated their added value for semi-distributed rainfall-runoff
728 model calibration. Continuous time series of near-surface soil water storage CRNS (S_{NS})
729 estimates at a landscape-representative location provide valuable information for improving
730 subsurface parameterization in regional land surface models (Baatz et al., 2017) or rainfall-
731 runoff model calibration (Dimitrova-Petrova et al., 2020a). This value can be enhanced if
732 combined with “snapshots” of near-surface wetness variability from portable CRNS surveys,
733 as demonstrated by Franz *et al.*, (2015) and McJannet *et al.*, (2017) from large scale
734 experiments in dry climates. Our combined approach was applied at the small catchment
735 scale to obtain continuous timeseries for different SLU units. It allowed identification of sites
736 with wetter or more variable SWC dynamics, which can be missed if solely a landscape

737 average SWC value is used to characterise catchment S-Q relationships (Mittelbach &
738 Seneviratne, 2012). The differences in near-surface soil water storage (S_{NS}) between
739 mineral and organic-rich SLU units were captured by the combined CRNS approach and
740 adequately constrained using an additional calibration of the N-SWC relationship.

741 While Dimitrova-Petrova et al., (2020a) previously demonstrated the value of the static
742 CRNS S_{NS} data in lumped rainfall-runoff model for Elsick, here we have expanded this to
743 semi-distributed applications. Although not directly comparable (i.e. the calibration period in
744 the present study was one year longer), the KGE median and ranges for discharge were
745 similar using either the lumped or the semi-distributed HBV-light model set-up. However, in
746 the semi-distributed approach here, the simulated discharge was better constrained as
747 compared to using solely discharge or discharge and S_{NS_static} and the internal catchment
748 storage dynamics are arguably better represented. The S_{NS_static} in the lumped model set-up
749 did yield higher goodness of fit measures, but this could be simply related to the higher
750 parameter uncertainty in the semi-distributed model due to having 36 parameters versus 15
751 in the lumped model set-up.

752 Ultimately, we have shown that CRNS technology provides a useful tool for semi-distributed,
753 as well as lumped, rainfall-runoff modelling; and that the set-up will depend on whether the
754 application requires a semi-distributed approach or not. Here, the semi-distributed HBV-light
755 rainfall-runoff model served as a learning tool to investigate the role of near- surface storage
756 and its spatiotemporal variation in the catchment-scale S-Q relationship. While the
757 importance of S_{NS} was evidenced by the improved model internal dynamics through the
758 combined calibration (Dimitrova Petrova et al., 2020a), the additional effort associated with
759 the combined static and portable CRNS approach for rainfall-runoff modelling yielded a
760 relatively small gain in terms of simulated discharge. In this predominantly agricultural
761 landscape, where land use managements (e.g. ploughing, artificial drainage) homogenises
762 the soils at the near surface, data from the static CRNS installed at a landscape-

representative location appeared to sufficiently inform catchment-scale S_{NS} dynamics (as demonstrated in Dimitrova- Petrova *et al.*, (2020a)).

Further testing of the method in environments with contrasting climates and where spatial heterogeneity in S_{NS} is more apparent will help evaluate whether deploying solely a static CRNS at a representative location in a catchment is sufficient or the combined approach could help to better characterise near-surface storage spatial heterogeneities. Another recommendation would be to test the use of CRNS in rainfall-runoff modelling in catchments with more pronounced seasonality. Such applications could help evaluate the trade-offs between the variable sensing depth of CRNS (Baroni et al., 2018; Peterson et al., 2016) and the usefulness of near-surface storage data to characterise catchment storage dynamics and potentially improve flood forecasting (Massari et al., 2014; Massari et al., 2018). Although not yet applied to hydrological modelling, similar but more data intense CRNS studies in drier agricultural landscapes (Gibson & Franz, 2018; McJannet et al., 2017) have successfully assessed spatiotemporal dynamics of near-surface storage. While distributed soil management poses additional challenges in mixed-agricultural environments, a combined CRNS approach complemented with a few continuous point-profile measurements could help elucidate the wider applicability of the approach and increase its information value along the SWC profile (Scheiffele et al., 2020). In addition, more complex models more sensitive to storage might benefit even more from the spatially variable S_{NS} information produced using the combined static and portable CRNS data approach.

5. Conclusions

We combined static and portable CRNS sensors to assess the spatial variability of near-surface soil water storage dynamics in a small ($10km^2$) humid mixed-agricultural catchment. For that, we developed and tested a method suited to this environment, which extends the information content of static CRNS to key soil-land use units. We demonstrated that the

789 approach worked well to characterise SWC dynamics at all key SLU units in the Elsick study
790 catchment, although recommend careful consideration of additional SWC calibration data
791 that accounts for spatial variability in depth as well as within the CRNS footprint. Within our
792 approach we also addressed landscape-specific CRNS related challenges. Firstly, much
793 longer integration time of neutron counts (~4 hours), compared to temperate and semi-arid
794 sites, were needed to account for high neutron uncertainty. Secondly, this study identified
795 the need for additional parameter calibration of the SWC CRNS function for characterising
796 SLU units with contrasting soil hydraulic properties. Here this involved the Moorland on
797 organic-rich poorly drained soils, typical for this and many other humid landscapes. We then
798 tested the value of the new spatially variable SWC catchment data for the catchment for a
799 semi-distributed rainfall-runoff model calibration, in comparison to simulations using just the
800 static CRNS data in a previous study. Based on minimal differences in model efficiency and
801 simulated runoff we conclude that (i) data from static CRNS at a landscape-representative
802 location might suffice to inform rainfall-runoff modelling at the small (1-10 km^2) catchment
803 scale (ii) depending on the research needs and objectives a (semi-)distributed model
804 structure might be useful in heterogeneous environments, but not strictly necessary. This
805 preliminary study shows the potential of combining CRNS technologies to assess
806 spatiotemporal variability of near-surface water storage in humid agricultural landscapes. It
807 also encourages further investigations in environments with contrasting climate or
808 pronounced seasonality to improve its accuracy and applicability. Depending on model
809 structure and the degree to which near-surface storage dynamics vary within the landscape,
810 such datasets can improve storage-discharge relationships, flood and agricultural
811 management applications in humid landscapes.

812

Acknowledgements

We thank the Macaulay Development Trust and School of Geosciences, University of Aberdeen for KDP's scholarship. JG would like to acknowledge funding from the Royal Society (RG140402), the Carnegie Trust for the Universities of Scotland (project 70112) and the UK Natural Environment Research Council (project NE/N007611/1 and CC13_080). RR received funding from the Natural Environment Research Council (projects NE/M003086/1, NE/ R004897/1 and NE/T005645/1) and from the International Atomic Energy Agency of the United Nations (IAEA/UN) (project CRP D12014). MW and AL were funded by the Rural & Environment Science & Analytical Services Division of the Scottish Government. We thank Lucile Verrot for helping with the depth-distance weighting of soil moisture. We thank to Hydroinnova for making available the solar intensity data from Jungfraujoch to us. Special thanks to Jessica Fennell, Lucile Verrot and Mark Grundy for assistance with fieldwork as well as to David Finlay and his team for enabling land access in Elsick.

References

Baatz, R., Bogena, H. R., Hendricks Franssen, H. J., Huisman, J. A., Montzka, C., & Vereecken, H. (2015). An empirical vegetation correction for soil water content quantification using cosmic ray probes. *Water Resources Research*, *51*(4), 2030–2046. https://doi.org/10.1002/2014WR016443

Baatz, Roland, Franssen, H. J. H., Han, X., Hoar, T., Reemt Bogena, H., & Vereecken, H. (2017). Evaluation of a cosmic-ray neutron sensor network for improved land surface model prediction. *Hydrology and Earth System Sciences*, *21*(5), 2509–2530. https://doi.org/10.5194/hess-21-2509-2017

Baroni, G., Schei, L. M., Schrön, M., Ingwersen, J., & Oswald, S. E. (2018). Uncertainty , sensitivity and improvements in soil moisture estimation with cosmic-ray neutron sensing, *564*(July 2017), 873–887. https://doi.org/10.1016/j.jhydrol.2018.07.053

Baroni, G., Scheiffele, L. M., Schrön, M., Ingwersen, J., & Oswald, S. E. (2018). Uncertainty, sensitivity and improvements in soil moisture estimation with cosmic-ray neutron sensing. *Journal of Hydrology*, *564*(January), 873–887. https://doi.org/10.1016/j.jhydrol.2018.07.053

Bartalis, Z., Wagner, W., Naeimi, V., Hasenauer, S., Scipal, K., Bonekamp, H., … Anderson, C. (2007). Initial soil moisture retrievals from the METOP-A Advanced Scatterometer (ASCAT). *Geophysical Research Letters*, *34*(20), 5–9. https://doi.org/10.1029/2007GL031088

Bell, V. A., Kay, A. L., Jones, R. G., Moore, R. J., & Reynard, N. S. (2009). Use of soil data in a grid-based hydrological model to estimate spatial variation in changing flood risk across the UK. *Journal of Hydrology*, *377*(3–4), 335–350. https://doi.org/10.1016/j.jhydrol.2009.08.031

Blann, K. L., Anderson, J. L., Sands, G. R., & Vondracek, B. (2009). Effects of agricultural drainage on aquatic ecosystems: A review. *Critical Reviews in Environmental Science and Technology*, *39*(11), 909–1001. https://doi.org/10.1080/10643380801977966

Boelter, D. H. (1968). Important physical properties of peat materials. *3rd International Peat Congress , 18–23 Aug. 1968, Quebec, Canada, Dep. of Energy, Mines and Resources, Ottawa, Canada.*

Bogena, H. R., Huisman, J. A., Baatz, R., Hendricks Franssen, H. J., & Vereecken, H. (2013). Accuracy of the cosmic-ray soil water content probe in humid forest ecosystems: The worst case scenario. *Water Resources Research*, *49*(9), 5778–5791. https://doi.org/10.1002/wrcr.20463

Bogena, H. R., Montzka, C., Huisman, J. A., Graf, A., Schmidt, M., Stockinger, M., … Vereecken, H. (2018). The TERENO-Rur Hydrological Observatory: A Multiscale Multi-Compartment Research Platform for the Advancement of Hydrological Science. *Vadose Zone Journal*, *17*(1), 0. https://doi.org/10.2136/vzj2018.03.0055

Boland-Brien, S. J., Basu, N. B., & Schilling, K. E. (2014). Homogenization of spatial patterns of hydrologic response in artificially drained agricultural catchments. *Hydrological Processes*, *28*(19), 5010–5020. https://doi.org/10.1002/hyp.9967

Boorman, D. B., Hollis, J. M., & Lilly, A. (1995). Hydrology of soil types: a hydrologically-based classification of the soils of United Kingdom. *Institute of Hydrology Report*, (126), 146. https://doi.org/10.1029/98GL02804

Boorman, D., Brooks, M., Clarke, M., Cooper, H., & Cowan, N. (2018). *COSMOS-UK User guide*.

Brauer, C. C., Teuling, A. J., Torfs, P. J. J. F., & Uijlenhoet, R. (2013). Investigating storage-discharge relations in a lowland catchment using hydrograph fitting, recession analysis, and soil moisture data. *Water Resources Research*, *49*(7), 4257–4264. https://doi.org/10.1002/wrcr.20320

British Geological Survey. (2019). Geology of Britain viewer.

Brocca, L., Melone, F., Moramarco, T., Wagner, W., Naeimi, V., Bartalis, Z., & Hasenauer, S. (2010). Improving runoff prediction through the assimilation of the ASCAT soil moisture product. *Hydrology and Earth System Sciences*, *14*(10), 1881–1893. https://doi.org/10.5194/hess-14-1881-2010

Brocca, L., Tullo, T., Melone, F., Moramarco, T., & Morbidelli, R. (2012). Catchment scale soil moisture spatial-temporal variability. *Journal of Hydrology*, *422–423*, 63–75. https://doi.org/10.1016/j.jhydrol.2011.12.039

886 Brown, I. (2020). Challenges in delivering climate change policy through land use targets for
887 afforestation and peatland restoration. *Environmental Science and Policy*,
888 *107*(February), 36–45. https://doi.org/10.1016/j.envsci.2020.02.013

889 Bruneau, P., & Johnson, S. M. (2014). Scotland's peatland - definitions and information
890 resources. Scottish Natural Heritage Commissioned Report No 701., (701), 1–62.

891 Brunetti, G., Šimůnek, J., Bogena, H., Baatz, R., Huisman, J. A., Dahlke, H., & Vereecken,
892 H. (2019). On the Information Content of Cosmic-Ray Neutron Data in the Inverse
893 Estimation of Soil Hydraulic Properties. *Vadose Zone Journal*, *18*(1).
894 https://doi.org/10.2136/vzj2018.06.0123

895 Choi, M., Jacobs, J. M., & Cosh, M. H. (2007). Scaled spatial variability of soil moisture
896 fields. *Geophysical Research Letters*, *34*(1), 1–6.
897 https://doi.org/10.1029/2006GL028247

898 Chrisman, B., & Zreda, M. (2013). Quantifying mesoscale soil moisture with the cosmic-ray
899 rover. *Hydrology and Earth System Sciences*, *17*(12), 5097–5108.
900 https://doi.org/10.5194/hess-17-5097-2013

901 Cooper, H. M., Bennett, E., Blake, J., Blyth, E., Boorman, D., Cooper, E., … Trill, E. (2020).
902 COSMOS-UK: National soil moisture and hydrometeorology data for empowering UK
903 environmental science. *Earth System Science Data*, (October).
904 https://doi.org/https://doi.org/10.5194/essd-2020-287

905 Coopersmith, E. J., Cosh, M. H., & Daughtry, C. S. T. (2014). Field-scale moisture estimates
906 using COSMOS sensors: A validation study with temporary networks and Leaf-Area-
907 Indices. *Journal of Hydrology*, *519*(PA). https://doi.org/10.1016/j.jhydrol.2014.07.060

908 Davies, B. E. (1974). Loss-on-ignition as an estimate of soil organic matter. *Soil Science*
909 *Society of America Journal*, *38*, 150–151.

910 Desilets, D., Zreda, M., & Ferré, T. P. A. (2010). Nature's neutron probe: Land surface
911 hydrology at an elusive scale with cosmic rays. *Water Resources Research*, *46*(11), 1–
912 7. https://doi.org/10.1029/2009WR008726

913 Dimitrova-Petrova, K., Geris, J., Mark Wilkinson, E., Rosolem, R., Verrot, L., Lilly, A., &
914 Soulsby, C. (2020a). Opportunities and challenges in using catchment-scale storage
915 estimates from cosmic ray neutron sensors for rainfall-runoff modelling. *Journal of*
916 *Hydrology*, 124878. https://doi.org/10.1016/j.jhydrol.2020.124878

917 Dimitrova-Petrova, K., Geris, J., Mark Wilkinson, E., Rosolem, R., Verrot, L., Lilly, A., &
918 Soulsby, C. (2020b). Opportunities and challenges in using catchment-scale storage
919 estimates from cosmic ray neutron sensors for rainfall-runoff modelling. *Journal of*
920 *Hydrology*, 124878. https://doi.org/10.1016/j.jhydrol.2020.124878

921 Dimitrova-Petrova, K., Geris, J., Wilkinson, M. E., Lilly, A., & Soulsby, C. (2020). Using
922 isotopes to understand the evolution of water ages in disturbed mixed land-use
923 catchments. *Hydrological Processes*, *34*(4), 972–990.
924 https://doi.org/10.1002/hyp.13627

925 Dong, J., Ochsner, T. E., Zreda, M., Cosh, M. H., & Zou, C. B. (2014a). Calibration and
926 Validation of the COSMOS Rover for Surface Soil Moisture Measurement. *Vadose*
927 *Zone Journal*, *13*(4), vzj2013.08.0148. https://doi.org/10.2136/vzj2013.08.0148

928 Dong, J., Ochsner, T. E., Zreda, M., Cosh, M. H., & Zou, C. B. (2014b). Calibration and
929 Validation of the COSMOS Rover for Surface Soil Moisture Measurement. *Vadose*
930 *Zone Journal*, *13*(4), vzj2013.08.0148. https://doi.org/10.2136/vzj2013.08.0148

931 Duygu, M. B., & Akyürek, Z. (2019). Using Cosmic-Ray Neutron Probes in Validating
932 Satellite Soil Moisture Products and Land Surface Models. *Water*, *11*(7), 1362.
933 https://doi.org/10.3390/w11071362

Evans, J. G., Ward, H. C., Blake, J. R., Hewitt, E. J., Morrison, R., Fry, M., … Jenkins, A. (2016). Soil water content in southern England derived from a cosmic-ray soil moisture observing system - COSMOS-UK. *Hydrological Processes*, *4999*(August), 4987–4999. https://doi.org/10.1002/hyp.10929

Fersch, B., Jagdhuber, T., Schrön, M., Völksch, I., & Jäger, M. (2018). Synergies for Soil Moisture Retrieval Across Scales From Airborne Polarimetric SAR, Cosmic Ray Neutron Roving, and an In Situ Sensor Network. *Water Resources Research*, *54*(11). https://doi.org/https://doi.org/10.1029/2018WR023337

Fersch, Benjamin. (2020). A dense network of cosmic-ray neutron sensors for soil moisture observation in a pre-alpine headwater catchment in Germany. *Earth System Science Data*, (April). https://doi.org/https://doi.org/10.5194/essd-2020-48

Finkenbiner, C. E., Franz, T. E., & Gibson, J. (2019). Integration of hydrogeophysical datasets and empirical orthogonal functions for improved irrigation water management. *Precision Agriculture*, *20*, 78–100. https://doi.org/https://doi.org/10.1007/s11119-018-9582-5

Foolad, F., Franz, T. E., Wang, T., Gibson, J., Kilic, A., Allen, R. G., & Suyker, A. (2017). Feasibility analysis of using inverse modeling for estimating field-scale evapotranspiration in maize and soybean fields from soil water content monitoring networks, 1263–1277. https://doi.org/10.5194/hess-21-1263-2017

Franz, T. (2018). *Soil moisture Mapping with a POrtable Cosmic Ray Neutron Sensor IAEA-TECDOC-1845 Soil*.

Franz, T. E., Wang, T., Avery, W., Finkenbiner, C., & Brocca, L. (2015). Combined analysis of soil moisture measurements from roving and fixed cosmic ray neutron probes for multiscale real-time monitoring. *Geophysical Research Letters*, *42*(9), 3389–3396. https://doi.org/10.1002/2015GL063963

Franz, T. E., Zreda, M., Ferre, T. P. A., Rosolem, R., Zweck, C., Stillman, S., … Shuttleworth, W. J. (2012). Measurement depth of the cosmic ray soil moisture probe affected by hydrogen from various sources. *Water Resources Research*, *48*(8), 1–9. https://doi.org/10.1029/2012WR011871

Geris, J., Tetzlaff, D., Mcdonnell, J., & Soulsby, C. (2015). The relative role of soil type and tree cover on water storage and transmission in northern headwater catchments. *Hydrological Processes*, *29*(7), 1844–1860. https://doi.org/10.1002/hyp.10289

Gibson, J., & Franz, T. E. (2018a). Spatial prediction of near surface soil water retention functions using hydrogeophysics and empirical orthogonal functions. *Journal of Hydrology*, *561*, 372–383. https://doi.org/10.1016/j.jhydrol.2018.03.046

Gibson, J., & Franz, T. E. (2018b). Spatial prediction of near surface soil water retention functions using hydrogeophysics and empirical orthogonal functions. *Journal of Hydrology*, *561*, 372–383. https://doi.org/10.1016/j.jhydrol.2018.03.046

Gruszowski, K. E., Foster, I. D. L., Lees, J. A., & Charlesworth, S. M. (2003). Sediment sources and transport pathways in a rural catchment, Herefordshire, UK. *Hydrological Processes*, *17*(13), 2665–2681. https://doi.org/10.1002/hyp.1296

Guo, X., Fu, Q., Hang, Y., Lu, H., Gao, F., & Si, J. (2020). Spatial variability of soil moisture in relation to land use types and topographic features on hillslopes in the black soil (mollisols) area of northeast China. *Sustainability (Switzerland)*, *12*(9), 8–10. https://doi.org/10.3390/SU12093552

Gupta, H. V., Kling, H., Yilmaz, K. K., & Martinez, G. F. (2009). Decomposition of the mean squared error and NSE performance criteria: Implications for improving hydrological modelling. *Journal of Hydrology*, *377*(1–2), 80–91. https://doi.org/10.1016/j.jhydrol.2009.08.003

983 Gwak, Y., & Kim, S. (2017). Factors affecting soil moisture spatial variability for a humid
984 forest hillslope. *Hydrological Processes*, *31*(2), 431–445.
985 https://doi.org/10.1002/hyp.11039

986 Hall, D. G. M., Reeve, M. J., Thomasson, A. J., & Wright, V. F. (1977). *Water retention,*
987 *porosity and density of field soils. Soil survey Technical Monograph No. 9. Soil Survey*
988 *of England and Wales. Rothamsted Experimental Station.* Harpenden. England: Lawes
989 Agricultural Trust.

990 Hallett, P., Hall, R., Raffan, A., Braun, H., Russell, T., Lilly, A., … Ball, B. (2016). *Effect of*
991 *Soil Structure and Field Drainage on Water Quality and Flood Risk*.

992 Hannaford, J. (2015). Climate-driven changes in UK river flows: A review of the evidence.
993 *Progress in Physical Geography*, *39*(1), 29–48.
994 https://doi.org/10.1177/0309133314536755

995 Hawdon, A., McJannet, D., & Wallace, J. (2014). Calibration and correction procedures for
996 cosmic-ray neutron soil moisture probes located across Australia. *Water Resources*
997 *Research*, *50*(6), 5029–5043. https://doi.org/10.1002/2013WR015138

998 Heidbuchel, I., Guntner, A., & Blume, T. (2016). Use of cosmic-ray neutron sensors for soil
999 moisture monitoring in forests. *Hydrology and Earth System Sciences*, *20*(3), 1269–
1000 1288. https://doi.org/10.5194/hess-20-1269-2016

1001 Heistermann, M., Francke, T., Schrön, M., & Oswald, S. E. (2021). Spatio-temporal soil
1002 moisture retrieval at the catchment-scale using a dense network of cosmic-ray neutron
1003 sensors, (February), 1–35. https://doi.org/https://doi.org/10.5194/hess-2021-25

1004 Hooke, J. M. (1979). An analysis of the processes of river bank erosion. *Journal of*
1005 *Hydrology*, *42*, 39–62. https://doi.org/https://doi.org/10.1016/0022-1694(79)90005-2

1006 House, J. I., Orr, H. G., Clark, J. M., Gallego-Sala, A. V., Freeman, C., Prentice, I. C., &

1007 Smith, P. (2010). Climate change and the British Uplands: Evidence for decision-
1008 making. *Climate Research*, *45*(1), 3–12. https://doi.org/10.3354/cr00982

1009 Hundecha, Y., Parajka, J., & Viglione, A. (2020). Assessment of past flood changes across
1010 Europe based on flood-generating processes. *Hydrological Sciences Journal*, *00*(00),
1011 1–18. https://doi.org/10.1080/02626667.2020.1782413

1012 Hupet, F., & Vanclooster, M. (2002a). Intraseasonal dynamics of soil moisture variability
1013 within a small agricultural maize cropped field. *Journal of Hydrology*, *261*(1–4), 86–101.
1014 https://doi.org/10.1016/S0022-1694(02)00016-1

1015 Hupet, F., & Vanclooster, M. (2002b). Intraseasonal dynamics of soil moisture variability
1016 within a small agricultural maize cropped field. *Journal of Hydrology*, *261*(1–4), 86–101.
1017 https://doi.org/10.1016/S0022-1694(02)00016-1

1018 Hydroinnova. (2020). CRNS Suitcase probe.

1019 Iwema, J., Rosolem, R., Baatz, R., Wagener, T., & Bogena, H. R. (2015). Investigating
1020 temporal field sampling strategies for site-specific calibration of three soil moisture-
1021 neutron intensity parameterisation methods. *Hydrology and Earth System Sciences*,
1022 *19*(7), 3203–3216. https://doi.org/10.5194/hess-19-3203-2015

1023 Iwema, Joost, Rosolem, R., Rahman, M., Blyth, E., & Wagener, T. (2017). Land surface
1024 model performance using cosmic-ray and point-scale soil moisture measurements for
1025 calibration. *Hydrology and Earth System Sciences*, *21*(6), 2843–2861.
1026 https://doi.org/10.5194/hess-21-2843-2017

1027 Jakobi, J., Huisman, J. A., Vereecken, H., Diekkrüger, B., & Bogena, H. R. (2018). Cosmic
1028 Ray Neutron Sensing for Simultaneous Soil Water Content and Biomass Quantification
1029 in Drought Conditions. *Water Resources Research*, *54*(10), 7383–7402.
1030 https://doi.org/10.1029/2018WR022692

1031 Jakobi, Jannis, Huisman, J. A., Schrön, M., Fiedler, J., Brogi, C., Vereecken, H., & Bogena,
1032 H. R. (2020). Error Estimation for Soil Moisture Measurements With Cosmic Ray
1033 Neutron Sensing and Implications for Rover Surveys. *Frontiers in Water*, *2*(May), 1–15.
1034 https://doi.org/10.3389/frwa.2020.00010

1035 Kędzior, M., & Zawadzki, J. (2016). Comparative study of soil moisture estimations from
1036 SMOS satellite mission, GLDAS database, and cosmic-ray neutrons measurements at
1037 COSMOS station in Eastern Poland. *Geoderma*, *283*, 21–31.
1038 https://doi.org/10.1016/j.geoderma.2016.07.023

1039 Lilly, A., Dunn, S. M., & Baggaley, N. J. (2012). *Hydrological Classifications of Soils and their*
1040 *Use in Hydrological Modeling*. *Hydropedology*. Elsevier B.V.
1041 https://doi.org/10.1016/B978-0-12-386941-8.00017-4

1042 Lilly, Allan, Baggaley, N., Rees, B., Topp, K., Dickson, I., & Elrick, G. (2012). Report on
1043 agricultural drainage and greenhouse gas abatement in Scotland. *The James Hutton*
1044 *Institute*, (November), 1–41.

1045 Lilly, Allan, Miller, D., Towers, W., Donnelly, D., Poggio, L., & Carnegie, P. (2015).
1046 MAPPING SCOTLAND ' S SOIL RESOURCES, *48*(Figure 2), 35–46.

1047 Lindström, G., Johansson, B., Persson, M., Gardelin, M., & Bergström, S. (1997).
1048 Development and test of the distributed HBV-96 hydrological model. *Journal of*
1049 *Hydrology*, *201*(1–4), 272–288. https://doi.org/10.1016/S0022-1694(97)00041-3

1050 Lv, L., Liao, K., Lai, X., Zhu, Q., & Zhou, S. (2016). Hillslope soil moisture temporal stability
1051 under two contrasting land use types during different time periods. *Environmental Earth*
1052 *Sciences*, *75*(7), 1–11. https://doi.org/10.1007/s12665-015-5238-1

1053 Marsh, C. B., Pomeroy, J. W., & Wheater, H. S. (2020). The Canadian Hydrological Model
1054 (CHM) v1.0: a multi-scale, multi-extent, variable-complexity hydrological model - design

and overview. *Geoscientific Model Development*, *13*(1), 225–247. https://doi.org/10.5194/gmd-13-225-2020

Massari, C, Brocca, L., Barbetta, S., Papathanasiou, C., Mimikou, M., & Moramarco, T. (2014). Using globally available soil moisture indicators for flood modelling in Mediterranean catchments, 839–853. https://doi.org/10.5194/hess-18-839-2014

Massari, Christian, Camici, S., Ciabatta, L., & Brocca, L. (2018). Exploiting Satellite-Based Surface Soil Moisture for Flood Forecasting in the Mediterranean Area : State Update Versus Rainfall Correction. https://doi.org/10.3390/rs10020292

Mcbride, A., Quin, J., Heritage, S. N., & Management, F. (2017). *What are the benefits of peatlands and their role in future farming systems?* Retrieved from https://www.nature.scot/peatland-action-poster-what-are-benefits-peatlands-and-their-role-future-farming-under-changing

Mccabe, M. F., Rodell, M., Alsdorf, D. E., Miralles, D. G., Uijlenhoet, R., Wagner, W., … Wood, E. F. (2017). The Future of Earth Observation in Hydrology, (February), 1–55. https://doi.org/10.5194/hess-2017-54

McJannet, D., Hawdon, A., Baker, B., Renzullo, L., & Searle, R. (2017). Multiscale soil moisture estimates using static and roving cosmic-ray soil moisture sensors. *Hydrology and Earth System Sciences*, *21*(12), 6049–6067. https://doi.org/10.5194/hess-21-6049-2017

McKay, M. D. (1992). Latin hypercube sampling as a tool in uncertainty analysis of computer models. *WSC '92: Proceedings of the 24th Conference on Winter Simulation*, *December*, 557–564. https://doi.org/https://doi.org/10.1145/167293.167637

Met Office. (2019a). MIDAS: UK Daily Rainfall Data. NCAS British Atmospheric Data Centre. 855.

1079 Met Office. (2019b). MIDAS: UK Daily Temperature Data. NCAS British Atmospheric Data
1080 Centre. 857.

1081 Meyles, E. W., Williams, A. G., Ternan, J. L., & Anderson, J. M. (2001). Effects of grazing on
1082 soil properties and hydrology of a small Dartmoor catchment, southwest England.
1083 *IAHS-AISH Publication*, (268), 279–286.

1084 Meyles, E., Williams, A., Ternan, L., & Dowd, J. (2003). Runoff generation in relation to soil
1085 moisture patterns in a small Dartmoor catchment, Southwest England. *Hydrological*
1086 *Processes*, *17*(2), 251–264. https://doi.org/10.1002/hyp.1122

1087 Mittelbach, H., & Seneviratne, S. I. (2012). A new perspective on the spatio-temporal
1088 variability of soil moisture : temporal dynamics versus time-invariant contributions,
1089 2169–2179. https://doi.org/10.5194/hess-16-2169-2012

1090 Montzka, C., Bogena, H., Zreda, M., Monerris, A., Morrison, R., Muddu, S., & Vereecken, H.
1091 (2017). Validation of Spaceborne and Modelled Surface Soil Moisture Products with
1092 Cosmic-Ray Neutron Probes. *Remote Sensing*, *9*(2), 103.
1093 https://doi.org/10.3390/rs9020103

1094 Nguyen, H. H., Kim, H., & Choi, M. (2017). Evaluation of the soil water content using cosmic-
1095 ray neutron probe in a heterogeneous monsoon climate-dominated region. *Advances in*
1096 *Water Resources*, *108*, 125–138. https://doi.org/10.1016/j.advwatres.2017.07.020

1097 O'Connell, P., Beven, K., Carney, J., Clements, R., Ewen, J., Fowler, H., … Tellier, S.
1098 (2004). *Review of Impacts of Rural Land Use and Management on Flood Generation.*
1099 *Impact Study Report. Appendix B*. Retrieved from http://evidence.environment-
1100 agency.gov.uk/FCERM/

1101 Ochsner, T. E., Linde, E., Haffner, M., & Dong, J. (2019). Mesoscale Soil Moisture Patterns
1102 Revealed Using a Sparse In Situ Network and Regression Kriging. *Water Resources*

Research, *55*(6), 4785–4800. https://doi.org/10.1029/2018WR024535

Pachepsky, Y., & Hill, R. L. (2017). Scale and scaling in soils. *Geoderma*, *287*, 4–30. https://doi.org/10.1016/j.geoderma.2016.08.017

Penna, D., Brocca, L., Borga, M., & Dalla Fontana, G. (2013). Soil moisture temporal stability at different depths on two alpine hillslopes during wet and dry periods. *Journal of Hydrology*, *477*, 55–71. https://doi.org/10.1016/j.jhydrol.2012.10.052

Percy, M. S., Riveros-Iregui, D. A., Mirus, B. B., & Benninger, L. K. (2020). Temporal and spatial variability of shallow soil moisture across four planar hillslopes on a tropical ocean island, San Cristóbal, Galápagos. *Journal of Hydrology: Regional Studies*, *30*(April), 100692. https://doi.org/10.1016/j.ejrh.2020.100692

Peters-Lidard, C.D., Pan, F., & Wood, E. F. (2001). A re-examination of modeled and measured soil moisture spatial variability and its implications for land surface modeling. *Advances in Water Resources*, *24*, 1069–1083. https://doi.org/https://doi.org/10.1016/S0309-1708(01)00035-5

Peters-Lidard, Christa D., Clark, M., Samaniego, L., Verhoest, N. E. C., Van Emmerik, T., Uijlenhoet, R., … Woods, R. (2017). Scaling, similarity, and the fourth paradigm for hydrology. *Hydrology and Earth System Sciences*, *21*(7), 3701–3713. https://doi.org/10.5194/hess-21-3701-2017

Peterson, A. M., Helgason, W. D., & Ireson, A. M. (2016). Estimating field-scale root zone soil moisture using the cosmic-ray neutron probe. *Hydrology and Earth System Sciences*, *20*(4), 1373–1385. https://doi.org/10.5194/hess-20-1373-2016

Rasche, D., Köhli, M., Schrön, M., Blume, T., & Güntner, A. (2021). Towards disentangling heterogeneous soil moisture patterns in Cosmic-Ray Neutron Sensor footprints, (April), 1–33.

Rinderer, M., & Seibert, J. (2012). *Soil Information in Hydrologic Models: Hard Data, Soft Data, and the Dialog between Experimentalists and Modelers*. *Hydropedology*. Elsevier B.V. https://doi.org/10.1016/B978-0-12-386941-8.00016-2

Rivera Villarreyes, C. A., Baroni, G., & Oswald, S. E. (2011). Integral quantification of seasonal soil moisture changes in farmland by cosmic-ray neutrons. *Hydrology and Earth System Sciences*, *15*(12), 3843–3859. https://doi.org/10.5194/hess-15-3843-2011

Rivera Villarreyes, C. A., Baroni, G., & Oswald, S. E. (2014). Inverse modelling of cosmic-ray soil moisture for field-scale soil hydraulic parameters. *European Journal of Soil Science*, *65*(6), 876–886. https://doi.org/10.1111/ejss.12162

Rosenbaum, U., Bogena, H. R., Herbst, M., Huisman, J. A., Peterson, T. J., Weuthen, A., … Vereecken, H. (2012). Seasonal and event dynamics of spatial soil moisture patterns at the small catchment scale. *Water Resources Research*, *48*(10), 1–22. https://doi.org/10.1029/2011WR011518

Rosolem, R., Gupta, H. V., Shuttleworth, W. J., Zeng, X., & De Gonçalves, L. G. G. (2012). A fully multiple-criteria implementation of the Sobol' method for parameter sensitivity analysis. *Journal of Geophysical Research Atmospheres*, *117*(7), 1–18. https://doi.org/10.1029/2011JD016355

RSPB. (2020). Farmin and crofting for wildlife: Grip blocking. Retrieved 7 July 2020, from https://www.rspb.org.uk/our-work/conservation/conservation-and-sustainability/farming/advice/techniques-to-help-wildlife/moorland-gripping/

Scheiffele, L. M., Baroni, G., Franz, T. E., Jakobi, J., & Oswald, S. E. (2020). A profile shape correction to reduce the vertical sensitivity of cosmic-ray neutron sensing of soil moisture. *Vadose Zone Journal*, (October), 1–25. https://doi.org/10.1002/vzj2.20083

Schreiner-McGraw, A. P., Vivoni, E. R., Mascaro, G., & Franz, T. E. (2016). Closing the

water balance with cosmic-ray soil moisture measurements and assessing their relation to evapotranspiration in two semiarid watersheds. *Hydrology and Earth System Sciences*, *20*(1), 329–345. https://doi.org/10.5194/hess-20-329-2016

Schrön, M., Rosolem, R., Köhli, M., Piussi, L., Schröter, I., Iwema, J., … Zacharias, S. (2018). Cosmic-ray Neutron Rover Surveys of Field Soil Moisture and the Influence of Roads. *Water Resources Research*, *54*(9), 6441–6459. https://doi.org/10.1029/2017WR021719

Schrön, Martin, Köhli, M. O., Schrön, M., Köhli, M., Scheiffele, L., Iwema, J., … Lv, L. (2017). Improving calibration and validation of cosmic-ray neutron sensors in the light of spatial sensitivity Improving Calibration and Validation of Cosmic-Ray Neutron Sensors in the Light of Spatial Sensitivity – Theory and Evidence, (October). https://doi.org/10.5194/hess-2017-148

Schrön, Martin, Köhli, M., Scheiffele, L., Iwema, J., Bogena, H. R., Lv, L., … Rebmann, C. (2017). Improving calibration and validation of cosmic-ray neutron sensors in the light of spatial sensitivity, 5009–5030.

Schrön, Martin, Köhli, M., Scheiffele, L., Iwema, J., Bogena, H. R., Lv, L., … Zacharias, S. (2017). Improving Calibration and Validation of Cosmic-Ray Neutron Sensors in the Light of Spatial Sensitivity – Theory and Evidence. *Hydrology and Earth System Sciences Discussions*, (March), 1–30. https://doi.org/10.5194/hess-2017-148

Seibert, J., & Vis, M. J. P. (2012). Teaching hydrological modeling with a user-friendly catchment-runoff-model software package. *Hydrology and Earth System Sciences*, *16*(9), 3315–3325. https://doi.org/10.5194/hess-16-3315-2012

Seibert, Jan, Bishop, K., Nyberg, L., & Rodhe, A. (2011). Water storage in a till catchment. I: Distributed modelling and relationship to runoff. *Hydrological Processes*, *25*(25), 3937–3949. https://doi.org/10.1002/hyp.8309

Shi, Y., Baldwin, D. C., Davis, K. J., Yu, X., Duffy, C. J., & Lin, H. (2015). Simulating high-resolution soil moisture patterns in the Shale Hills watershed using a land surface hydrologic model. *Hydrological Processes*, *29*(21), 4624–4637. https://doi.org/10.1002/hyp.10593

Sigouin, M. J. P., Dyck, M., Cheng Si, B., & Hu, W. (2016). Monitoring soil water content at a heterogeneous oil sand reclamation site using a cosmic-ray soil moisture probe. *Journal of Hydrology*, *543*, 510–522. https://doi.org/10.1016/j.jhydrol.2016.10.026

Soil Survey of Scotland Staff. (1981). *Soil maps of Scotland at a scale of 1:250 000. Macaulay Institute for Soil Research, Aberdeen*.

Stevanato, L., Baroni, G., Cohen, Y., Lino, F. C., Gatto, S., Lunardon, M., … Morselli, L. (2019). A novel cosmic-ray neutron sensor for soil moisture estimation over large areas. *Agriculture (Switzerland)*, *9*(9). https://doi.org/10.3390

Tetzlaff, D., Birkel, C., Dick, J., Geris, J., & Soulsby, C. (2014). Storage dynamics in hydropedological units control hillslope connectivity, runoff generation, and the evolution of catchment transit time distributions. *Water Resources Research*, *50*(2), 969–985. https://doi.org/10.1002/2013WR014147

Tetzlaff, D., Soulsby, C., Waldron, S., Malcolm, I. A., Bacon, P. J., Dunn, S. M., … Youngson, A. F. (2007). Conceptualization of runoff processes using a geographical information system and tracers in a nested mesoscale catchment. *Hydrological Processes*, *21*(10), 1289–1307. https://doi.org/10.1002/hyp.6309

Tetzlaff, Doerthe, Buttle, J., Carey, S. K., van Huijgevoort, M. H. J., Laudon, H., Mcnamara, J. P., … Soulsby, C. (2015). A preliminary assessment of water partitioning and ecohydrological coupling in northern headwaters using stable isotopes and conceptual runoff models. *Hydrological Processes*, *29*(25), 5153–5173. https://doi.org/10.1002/hyp.10515

Vachaud, G., Passerat De Silans, A., Balabanis, P., & Vauclin, M. (1985). Temporal stability of spatially measured soil water probability density function. *Soil Science Society of America Journal*, *49*, 822–828. https://doi.org/https://doi.org/10.2136/sssaj1985.03615995004900040006x

Vaezi, A. R., Zarrinabadi, E., & Auerswald, K. (2017). Interaction of land use, slope gradient and rain sequence on runoff and soil loss from weakly aggregated semi-arid soils. *Soil and Tillage Research*, *172*(May), 22–31. https://doi.org/10.1016/j.still.2017.05.001

Vanderlinden, K., Vereecken, H., Hardelauf, H., Herbst, M., Martínez, G., Cosh, M. H., & Pachepsky, Y. A. (2012). Temporal Stability of Soil Water Contents: A Review of Data and Analyses. *Vadose Zone Journal*, *11*(4), 0. https://doi.org/10.2136/vzj2011.0178

Vather, T., Everson, C., & Franz, T. E. (2019). Calibration and Validation of the Cosmic Ray Neutron Rover for Soil Water Mapping within Two South African Land Classes. *Hydrology*, *6*(3), 65. https://doi.org/10.3390/hydrology6030065

Vather, T., Everson, C. S., & Franz, T. E. (2020). The Applicability of the Cosmic Ray Neutron Sensor to Simultaneously Monitor Soil Water Content and Biomass in an Acacia mearnsii Forest.

Vereecken, H., Huisman, J. A., Pachepsky, Y., Montzka, C., van der Kruk, J., Bogena, H., … Vanderborght, J. (2014). On the spatio-temporal dynamics of soil moisture at the field scale. *Journal of Hydrology*, *516*. https://doi.org/10.1016/j.jhydrol.2013.11.061

Verrot, L., & Destouni, G. (2016). Data-model comparison of temporal variability in long-term time series of large-scale soil moisture. *Journal of Geophysical Research*, *121*(17), 10056–10073. https://doi.org/10.1002/2016JD025209

Wallace, E. E., & Chappell, N. A. (2020). A statistical comparison of spatio-temporal surface moisture patterns beneath a semi-natural grassland and permanent pasture: From

drought to saturation. *Hydrological Processes*, *34*(13), 3000–3020. https://doi.org/10.1002/hyp.13774

Western, A. W., Zhou, S. L., Grayson, R. B., McMahon, T. A., Blöschl, G., & Wilson, D. J. (2004). Spatial correlation of soil moisture in small catchments and its relationship to dominant spatial hydrological processes. *Journal of Hydrology*, *286*(1–4), 113–134. https://doi.org/10.1016/j.jhydrol.2003.09.014

Withers, P. J. A., Hodgkinson, R. A., Bates, A., & Withers, C. L. (2007). Soil cultivation effects on sediment and phosphorus mobilization in surface runoff from three contrasting soil types in England. *Soil and Tillage Research*, *93*(2), 438–451. https://doi.org/10.1016/j.still.2006.06.004

Zhao, W., Cui, Z., & Zhou, C. (2020). Spatiotemporal variability of soil-water content at different depths in fields mulched with gravel for different planting years. *Journal of Hydrology*, 125253. https://doi.org/10.1016/j.jhydrol.2020.125253

Zhou, X., Lin, H., & Zhu, Q. (2007). Temporal stability of soil moisture spatial variability at two scales and its implication for optimal field monitoring. *Hydrology and Earth System Sciences Discussions*, *4*(3), 1185–1214. https://doi.org/10.5194/hessd-4-1185-2007

Zreda, M., Shuttleworth, W. J., Zeng, X., Zweck, C., Desilets, D., Franz, T., & Rosolem, R. (2012). COSMOS: The cosmic-ray soil moisture observing system. *Hydrology and Earth System Sciences*, *16*(11), 4079–4099. https://doi.org/10.5194/hess-16-4079-2012

Zreda, Marek, Desilets, D., Ferré, T. P. A., & Scott, R. L. (2008). Measuring soil moisture content non-invasively at intermediate spatial scale using cosmic-ray neutrons. *Geophysical Research Letters*, *35*(21), 1–5. https://doi.org/10.1029/2008GL035655

Zucco, G., Brocca, L., Moramarco, T., & Morbidelli, R. (2014a). Influence of land use on soil moisture spatial-temporal variability and monitoring. *Journal of Hydrology*, *516*, 193–

199. https://doi.org/10.1016/j.jhydrol.2014.01.043

Zucco, G., Brocca, L., Moramarco, T., & Morbidelli, R. (2014b). Influence of land use on soil moisture spatial-temporal variability and monitoring. *Journal of Hydrology*, *516*, 193–199. https://doi.org/10.1016/j.jhydrol.2014.01.043

Table 1. Distribution of soil-land use (SLU) classes in the Elsick catchment. In bold the classes represented by the $CRNS_{portable}$ sampling (covering 94% of the catchment).

Soil land use (SLU) class	**% $CRNS_{static}$**	**% Elsick**
Crop – Imperfectly drained (CropI) *Rotational crops on imperfectly drained podzols*	-	35%
Crop – Poorly drained (CropP) *Rotational crops on poorly drained gleys*	75%	32%
Pasture – Freely drained (PastureF) *Pasture on freely drained podzols*	25%	17%
Moorland- Poorly drained (MoorlandP) *Moorland and woodland on poorly drained peats and peaty podzols with organic-rich surface layer*	-	10%
Others (Forest plantations on mineral soils)	-	4%
Suburban and quarries	-	<2%
Open Water	-	<1%

Table 2. Initial parameter ranges of the two CRNS calibration approaches tested for deriving synthetic SWC_{SLU} timeseries from the combined CRNS dataset.

Calibration	N_0	a_0	a_1	a_2	Initial parameter range N_0	Initial parameter range a_i
Typical (SWC_{typ})	calibrated	fixed	fixed	fixed	-	Fixed a_0=0.0808 [cm^3 g^{-1}] a_1=0.372 [-] a_2=0.115 [cm^3 g^{-1}]
New (SWC_{new})	calibrated	calibrated	calibrated	calibrated	N_{0_static} = 3450 cph±10%	a_0= [0 1] [cm^3 g^{-1}] a_1=[0 1] [-] a_2=[0 1] [cm^3 g^{-1}]

1266

1267

1268

Table 3. Overview statistics (median, minimum and maximum) of the goodness of fit of the 50 best model runs. Both the multiple criteria $KGE_{multiple}$ as well as the individual KGE measures are presented.

	Goodness of fit Median [Min Max]	*Calib.target*
$KGE_{multiple}$	0.51 [0.49-0.52]	Multiple criteria (Eq. 7)
KGE_Q_{sim}	0.70 [0.63-0.74]	Q_{OUT}
$KGE\_S_{dyn\_PastureF}$	0.40 [0.25-0.49]	$S_{NS\_PastureF}$
$KGE\_S_{dyn\_CropI}$	0.36 [0.24-0.43]	S_{NS_CropI}
$KGE\_S_{dyn\_CropP}$	0.33 [0.25-0.42]	S_{NS_CropP}
$KGE\_S_{dyn\_MoorlandP}$	0.31 [0.22 - 0.37]	$S_{NS\_MoorlandP}$

Table 4. Overview of soil characteristics (bulk density ρ_{dry}, soil organic matter SOM and lattice water LW) and calibrated parameters using the typical or the new sensor calibration for each SLU unit. For the typical one, a_i parameters are fixed (a_0=0.0808, a_1=0.372 and a_2=0.115, Desilets et al., 2010). For the new calibration all four parameters are calibrated. RMSE (fit to field data) is also reported.

Soil Land Use Unit	ρ_{dry} [g cm^{-3}]	SOM + LW [m^3 m^{-3}]	Typical calibration	New (N_0 + a_i) calibration				
			N_0 [cph]	N_0 [cph]	a_0	a_1	a_2	RMSE [m^3 m^{-3}]
Static CRNS	1.09	0.07	3450 (1)	-	-	-	-	-
CropP	1.13	0.07	3510	3610	0.326	0.278	0.944	0.033
PastureF	0.98	0.07	3720	3214	0.521	0.194	0.83	0.035
CropI	1.1	0.07	3680	3490	0.076	0.432	0.202	0.014
MoorlandP	0.28	0.41	3910	4332	0.938	0.117	0.0974	0.006

Table 5. Overview statistics of near-surface soil water storage (S_{NS}) estimates from the static CRNS and individual SLU units (considered S_{NS} timeseries for rainfall-runoff modelling in bold).

S_{NS} (mm)	Static S_{NS_static}	CropP		PastureF		CropI		MoorlandP	
		Typ.	New	Typ.	New	Typ.	New	Typ.	New
Min	66	**44**	41	**70**	69	**48**	40	220	**222**
Mean	150	**164**	186	**204**	197	**164**	170	281	**271**
Median	151	**165**	202	**215**	205	**165**	173	292	**272**
Max	219	**240**	240	**240**	240	**240**	240	320	**305**
SD	27	**47**	51	**37**	36	**40**	43	35	**15**
NA	5	**37**	188	**6**	28	**5**	30	5	**5**

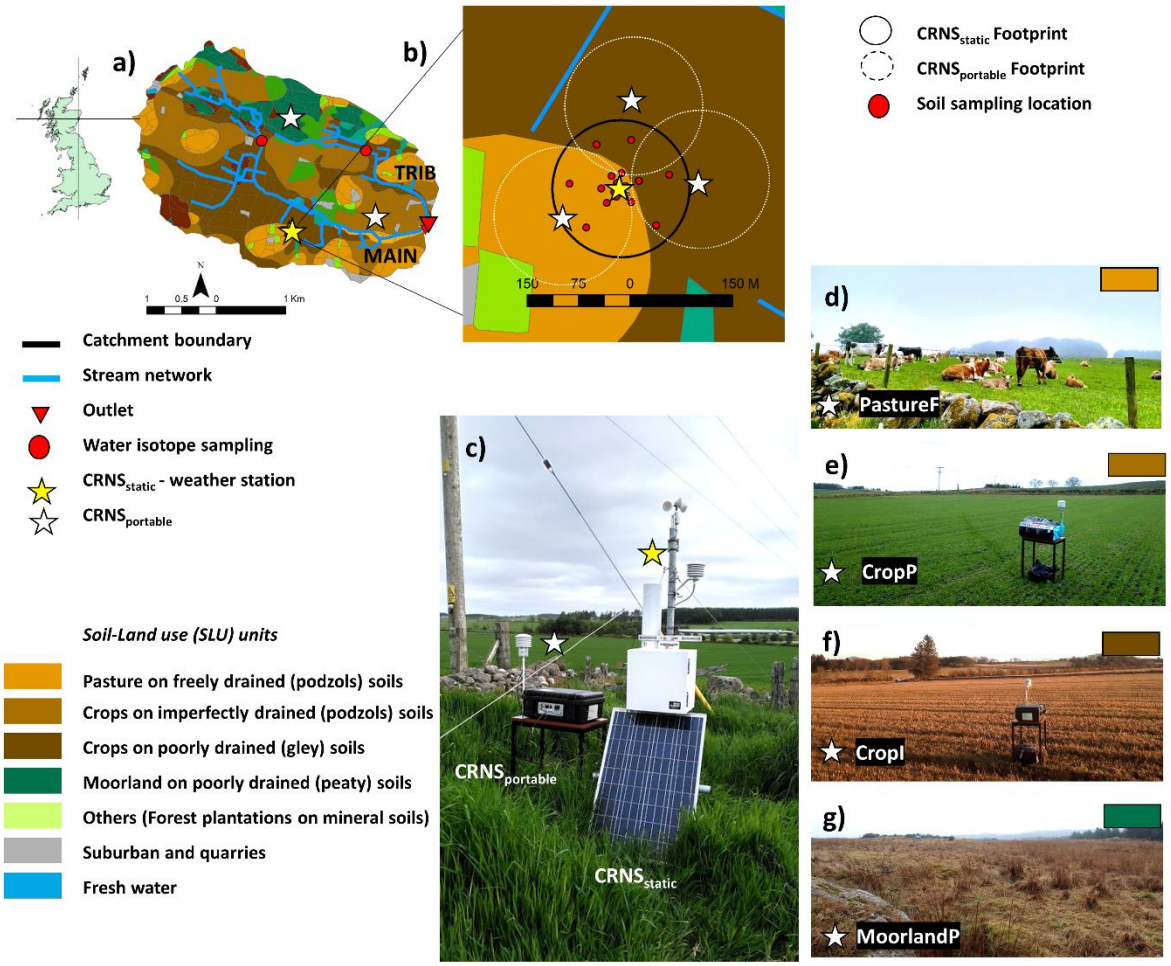

Figure 1. The Elsick catchment and instrumentation, showing (a) the soil-land use (SLU) units distribution and overview of the permanent and temporary monitoring infrastructure i.e. location of the gauging stations, CRNS$_{static}$ and CRNS$_{portable}$ sensor sampling; (b) zoom of the CRNS$_{static}$ location (yellow star) and footprint, covering two SLU units and soil sampling locations for sensor calibration. The white stars and circumference indicate the locations where portable CRNS was deployed and distributed topsoil (0-6 cm) SWC measurements were taken within its footprint; (c) the static (i.e. permanently installed) CRNS-weather station and portable CRNS; (d) to (g) show sampling locations of individual SLU units: (d) PastureF; (e) CropP; (f) CropI and (g) MoorlandP.

1298

1299

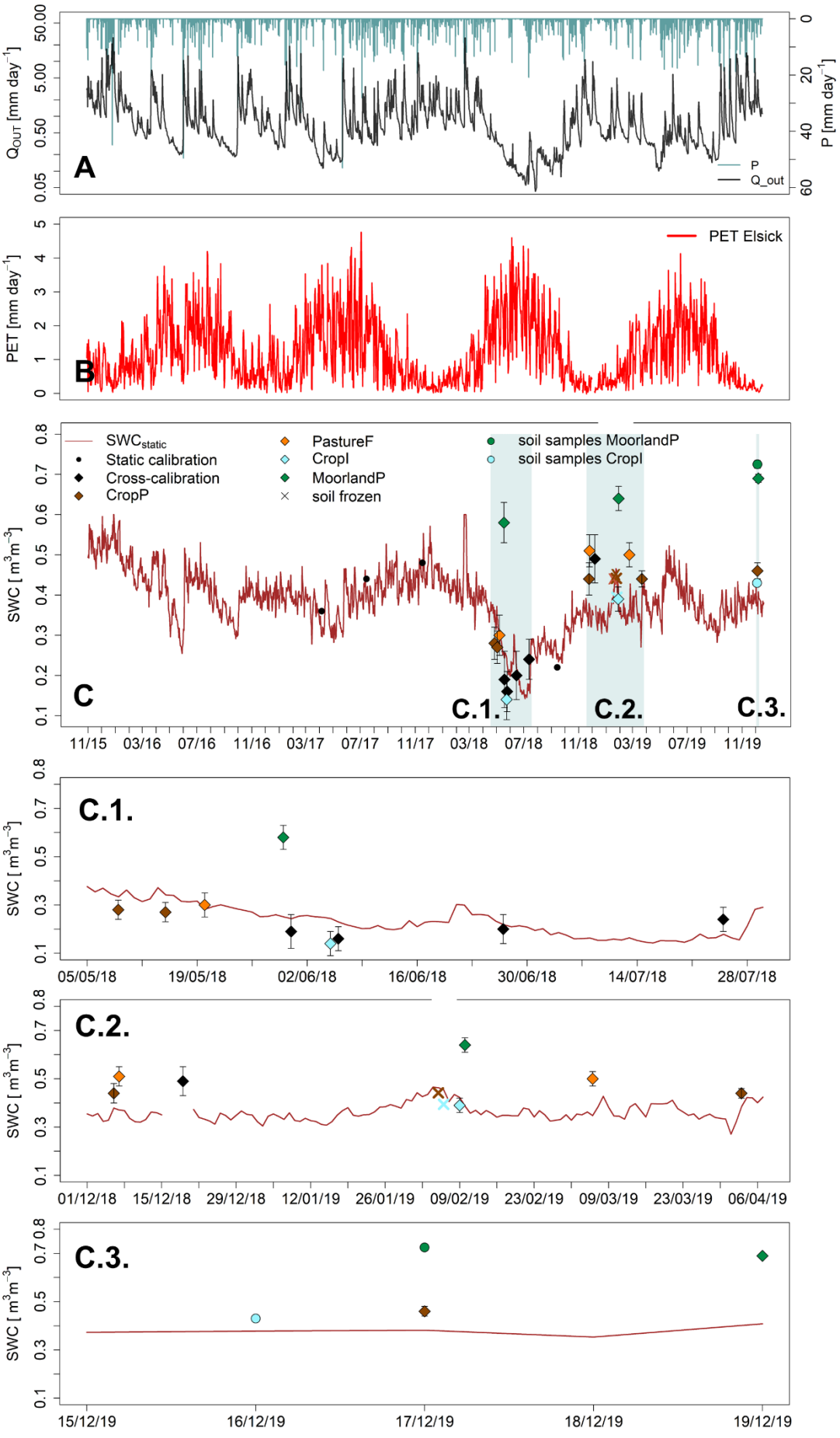
A
P
Q_out
B
PET Elsick
C
SWC_static
Static calibration
Cross-calibration
CropP
PastureF
CropI
MoorlandP
soil frozen
soil samples MoorlandP
soil samples CropI
C.1.
C.2.
C.3.
SWC [m3m-3]
11/15
03/16
07/16
11/16
03/17
07/17
11/17
03/18
07/18
11/18
03/19
07/19
11/19
05/05/18
19/05/18
02/06/18
16/06/18
30/06/18
14/07/18
28/07/18
01/12/18
15/12/18
29/12/18
12/01/19
26/01/19
09/02/19
23/02/19
09/03/19
23/03/19
06/04/19
15/12/19
16/12/19
17/12/19
18/12/19
19/12/19

Figure 2. Timeseries of P, Q_{OUT}, PET and SWC_{static} for the period 14 November 2015 to 31 December 2019. Panel C highlights in blue the three specific periods during which $CRNS_{portable}$ sampling took place. Daily depth-distance weighted averages of field SWC sampled using theta probe (diamond) or soil samples (circles) at each SLU unit are also shown, standard deviation (SD, as error bars) also shown. $CRNS_{static}$ calibration includes soil samples taken at the PastureF and CropP SLU units. Panels C1 to C3 zoom in those periods. Sampling days on which soils were frozen are indicated with X in panel C and C2.

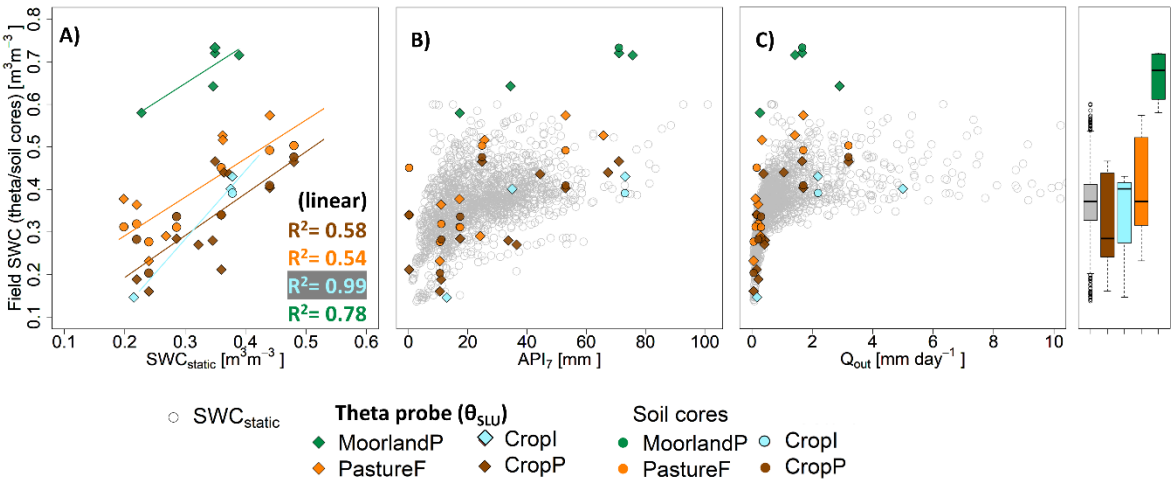

Figure 3. Overview of the relationships of topsoil SWC (either theta probe θ_{SLU} or soil cores information) the four SLU units to proxies of catchment wetness dynamics (a) SWC_{static}; (b) API_7 and (c) Q_{OUT}. Daily averages of SWC_{static} (grey circles) are also plotted against API_7 and Q_{OUT} (Figure 3 B and C, respectively) for context. Boxplots on the right-hand side illustrate the range of the field SWC data.

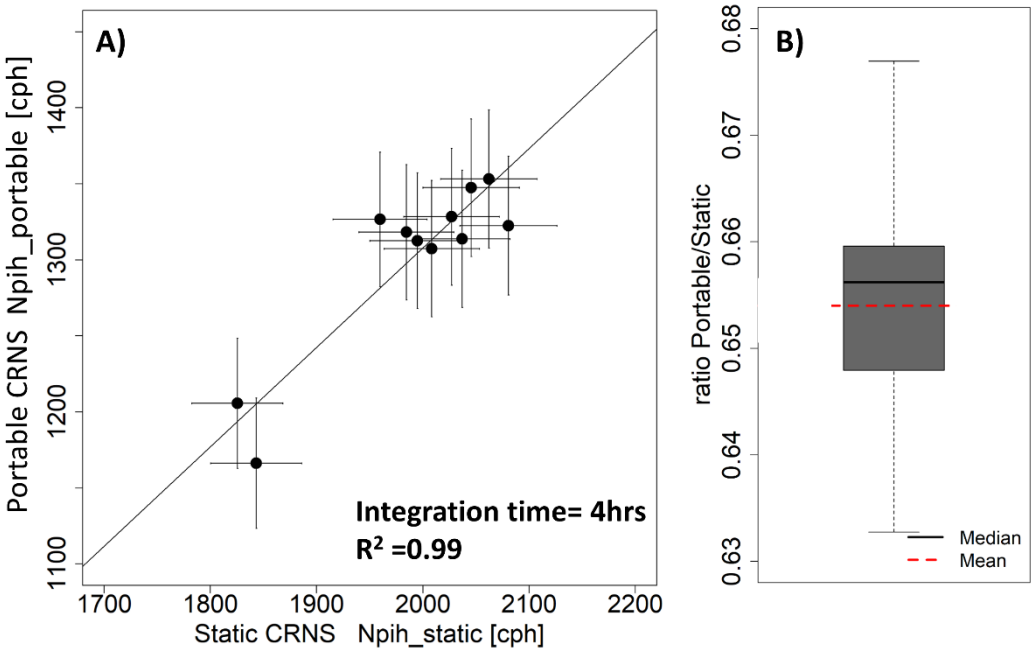

Figure 4. CRNS sensors cross-calibration A) Scatterplot showing correlation between the scaled corrected counts of portable CRNS ($Npih_{portable}$) versus static CRNS ($Npih_{static}$) within the footprint of the permanently installed sensor. B) Boxplots showing the spread of the ratio Portable/Static CRNS for 4hrs integration times and the mean of the ratios (0.654, in red) (median shown as the thick black line of the boxplot).

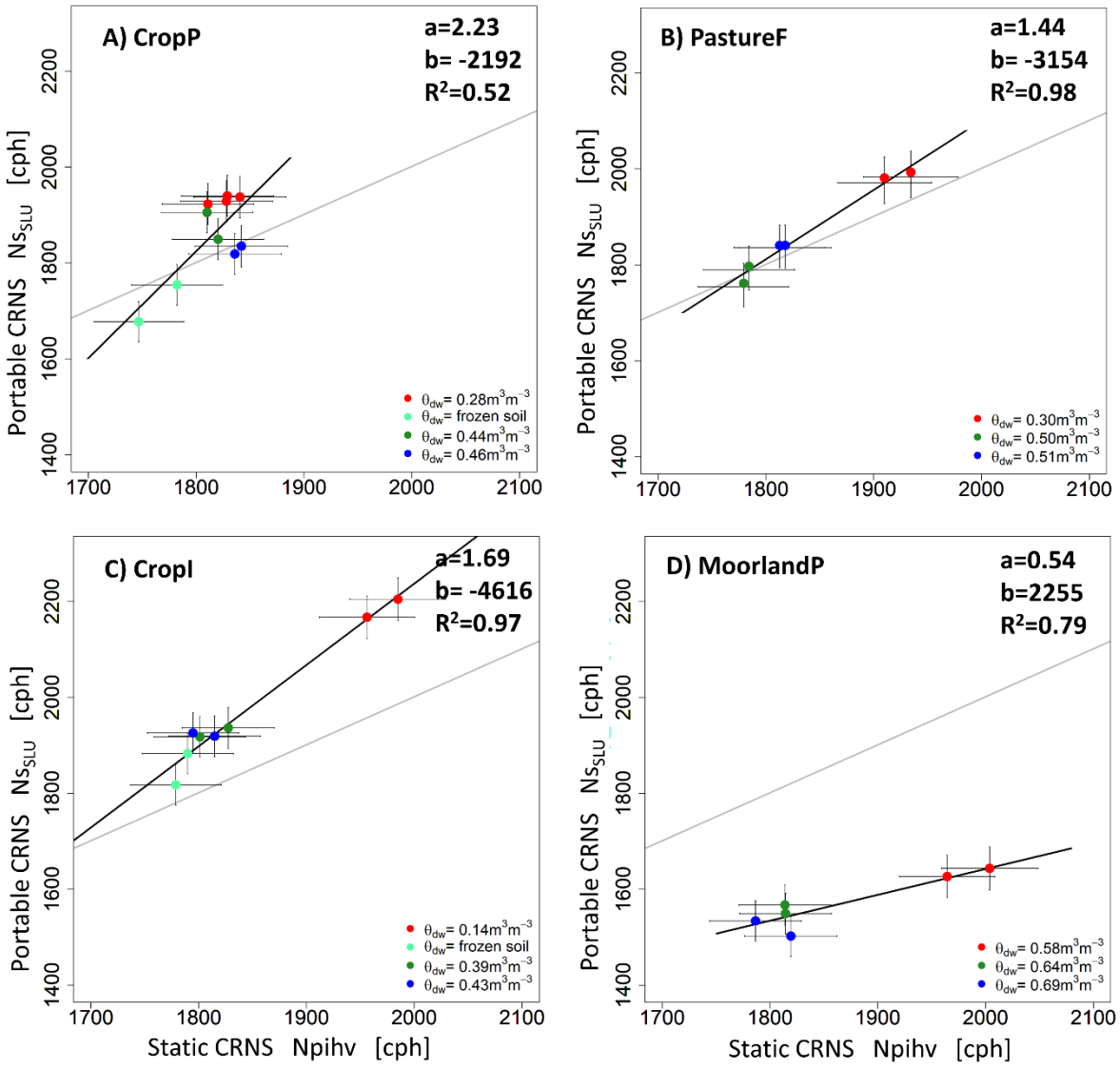

Figure 5. Relationship between static and portable CRNS data derived from neutron counts corrected for atmospheric influences, in the case of the portable (Ns_{SLU}) and additionally corrected for the effect of vegetation in the case of the static (Npihv).for integration times of 4h, all scaled to 1h (cph). Each subplot corresponds to an individual soil-land use unit. In brackets the weighted volumetric SWC (θdw in m^3 m^{-3}) measured in the field using the θ probe. The colours of the dots indicate whether the field soil moisture was considered dry (red), intermediate (green) or wet (dark blue) or if the topsoil was

frozen (light blue). Error bars correspond to the coefficient of variance (CV). Black line represents the trendline of the linear regression (y=ax+b). Grey line represents a 1:1 relationship.

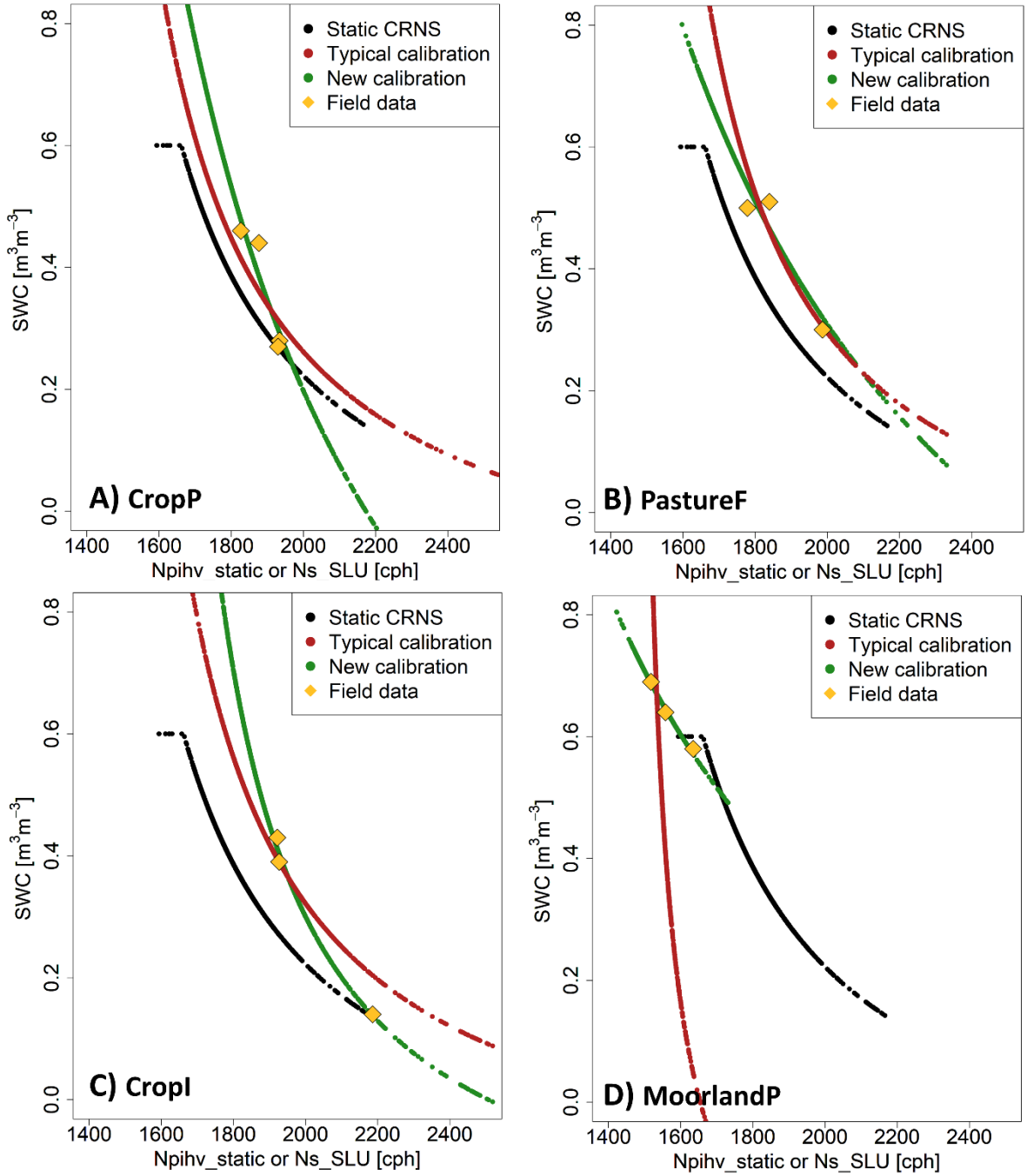

Figure 6. The $Npihv_{static}$-SWC relationship for the static CRNS (black) and the N_{s_SLU}-SWC synthetic timeseries, using typical (in red) and new (in green) sensor calibration together with the field data tested.

1341

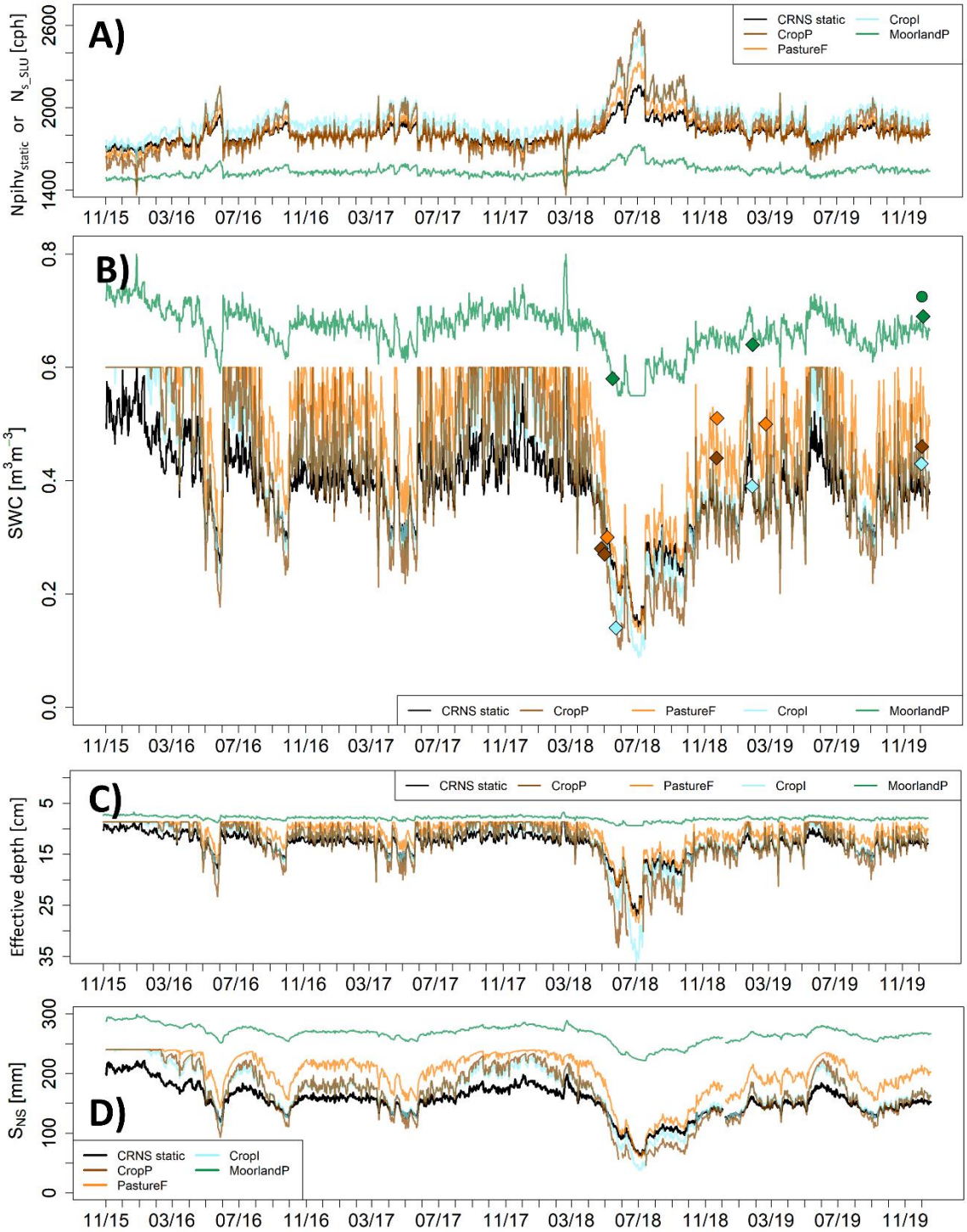

Figure 7. Portable SWC and related variables: overview A) Daily average Npihv for $CRNS_{static}$ and N_{s_SLU} for each individual SLU units. B) SWC for the $CRNS_{static}$ and synthetic estimates SWC_{SLU} of

individual SLU units; C) Effective depth (z_{eff}) of CRNS and estimates for individual SLU units; d) Estimated S_{NS} (in mm) for with $CRNS_{static}$ and S_{NS_SLU} for individual units..

1356

1357

1358

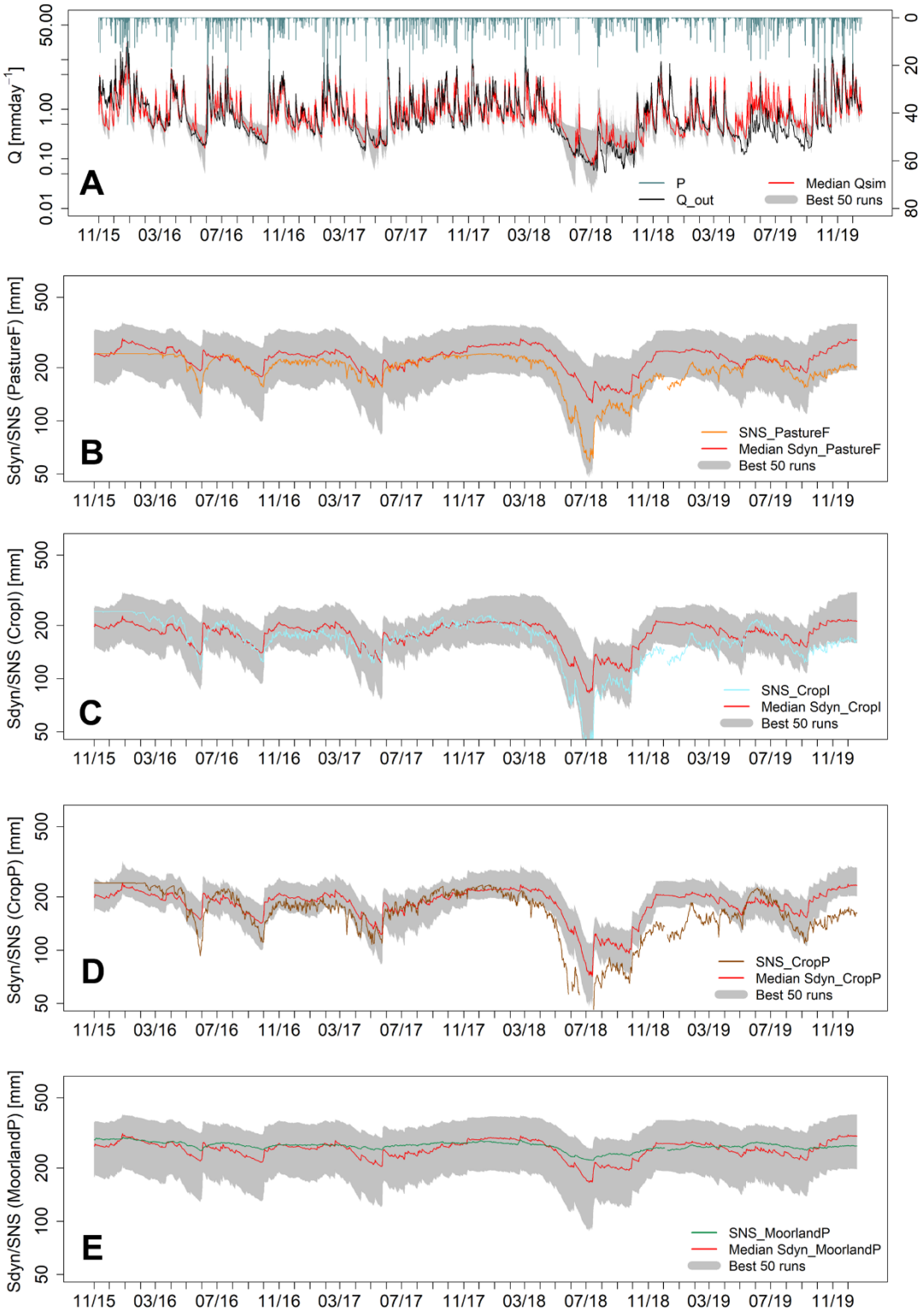
A
Q [mmday^{-1}]
50.00
1.00
0.10
0.01
0
20
40
60
80
P
Q_out
Median Qsim
Best 50 runs
11/15
03/16
07/16
11/16
03/17
07/17
11/17
03/18
07/18
11/18
03/19
07/19
11/19
B
Sdyn/SNS (PastureF) [mm]
500
200
100
50
SNS_PastureF
Median Sdyn_PastureF
Best 50 runs
C
Sdyn/SNS (CropI) [mm]
SNS_CropI
Median Sdyn_CropI
Best 50 runs
D
Sdyn/SNS (CropP) [mm]
SNS_CropP
Median Sdyn_CropP
Best 50 runs
E
Sdyn/SNS (MoorlandP) [mm]
SNS_MoorlandP
Median Sdyn_MoorlandP
Best 50 runs

1359

Figure 8. Semi-distributed rainfall-runoff modelling outcomes. Panel A show the time series of incoming precipitation P and the time series of observed Q_{OUT}, median (in red) and uncertainty bands (in grey) of Q_{sim} of the best 50 runs using a multiple-criteria calibration approach i.e. combining S_{NS_SLU} and Q_{OUT} as model calibration targets. Panel B to E show the simulated dynamic storage S_{dyn} and corresponding the S_{NS_SLU} data used for its calibration. The median (in red) and uncertainty bands (in grey) of the best 50 runs in also displayed. Pareto ranking of ($KGE_{multiple,}$ Eq. 7) used as a goodness of fit measure.

Appendix I Definitions of storage and related terms.

Abbreviation	Units	Definition	Reference
CRNS	[-]	Cosmic ray neutron sensor	Hydroinnova, New Mexico
$CRNS_{static}$	[-]	A static cosmic ray neutron sensor installed in a permanent location	This study
$CRNS_{portable}$	[-]	A portable cosmic ray neutron sensor which can be moved to different locations. Applications include rover (mounted on a vehicle), backpack (carried on a field operator's back). The current study uses the suitcase or cross-calibrator version of Hydroinnova.	(Dong et al., 2014; Franz, 2018; Hydroinnova, 2020)
N_{raw}	[cph]	Cosmic ray neutron intensity as measured by the CRNS, in neutron counts per hour [cph],	This study
Npih(v)	[cph]	Cosmic ray neutron intensity measured as neutron counts per hour [cph], inversely correlated to all hydrogen present in the upper decimetres of the subsurface and the first few hectometres of the atmosphere above the ground surface. The N signal is corrected for effects of atmospheric pressure (p), incoming neutron flux (i), air humidity (h) and in some cases the effect of aboveground vegetation (v)	(Baatz et al., 2015; Zreda et al., 2012; Zreda et al., 2008)
$Npihv_{static}$	[cph]	Npihv, as defined above, derived from data obtained with the static CRNS	(Baatz et al., 2015; Zreda et al., 2012; Zreda et al., 2008)
$Npih_{portable}$	[cph]	Npih, as defined above, derived from data obtained with the portable CRNS	(Baatz et al., 2015; Zreda et al., 2012; Zreda et al., 2008)
$N_{s\_portable}$	[cp4h]	$Npih_{portable}$ (up)scaled by a known ratio, so that portable matches the magnitude/potency of the static CRNS data. Used to define the relationship between portable and static CRNS data via linear regression	This study

N_{s_SLU} (t)	[cph]	Synthetically derived time series of neutron intensity derived for an individual soil-land use unit within the catchment, from time series of $Npih_{static}$, based on the linear relationship between $N_{s\_portable}$[cp4h] and $Npih_{static}$.	This study
z_{eff} (t)	[cm]	Estimated effective sensing depth of the CRNS at time t, a function of SWC, bulk density and soil organic matter (SOM)	(add ref from methods)
SWC_{static}	[m^3 m^{-3}]	Field average (~ 14 ha) soil water content based on calibrated static Cosmic Ray Neutron Sensor data; integrated over a time-variable sensing depth z_{eff} (between 0.07 and 0.2 m)	(Schrön et al., 2017; Zreda et al., 2008)
SWC_{typ}	[m^3 m^{-3}]	Synthetically derived time series of field average soil water content using a typical sensor calibration (N_0 parameter) for an individual soil-land use unit within the catchment; integrated over a time-variable sensing depth z_{eff}	This study
SWC_{new}	[m^3 m^{-3}]	Synthetically derived time series of field average soil water content using a new sensor calibration (N_0 and a_i parameters) for an individual soil-land use unit within the catchment; integrated over a time-variable sensing depth z_{eff}	This study
SWC_{SLU}	[m^3 m^{-3}]	Synthetically derived time series of field average soil water content for individual soil-land use unit within the catchment; integrated over a time-variable sensing depth z_{eff}. The SWC values are derived using either typical or new sensor calibration of the neutron intensity	This study
θ_{SLU}	[m^3 m^{-3}]	The arithmetic average of the theta θ probe measurements on each sampling day, used to characterise the CRNS signal and to account for point scale spatial variability of SWC within the footprint on that day	(Delta T Devices Ltd.)

S_{NS}	[mm]	Near-surface storage for a defined depth (z=0.4 m)	This study, (Dimitrova-Petrova et al., 2020a)
S_{NS_static}	[mm]	Near-surface storage for a defined depth (z=0.4 m) determined as the sum of SWC_{static} and SWC_{static}^{sub}	This study
S_{NS_SLU}	[mm]	Near-surface storage for a defined depth (z=0.4 m) determined as the sum of SWC_{SLU} and SWC_{SLU}^{sub}	This study
S_{dyn_SLU}	[mm]	Dynamic Storage(catchment scale), considered to control the majority of streamflow response. In the selected model structure set-up, it is the sum of the storage in the SM (soil moisture) and the SUZ (upper groundwater zone) boxes in the semi-distributed set-up of the HBV-light model. The indices correspond to the SLU units, data from which (S_{NS_SLU}) was used to calibrate each of the four dynamic storage boxes.	This study
SM	[mm]	HBV model: Soil moisture box with its largest value equal to FC (field capacity). Partitioning of rainfall in soil water content and groundwater recharge. Does not produce runoff	(Seibert, 2005)
SUZ	[mm]	HBV model: Upper groundwater box, recharged by the SM box. Faster runoff (Q_0) of the SUZ box depends on the UZL (upper zone limit) parameter which acts as a threshold above which runoff is produced. Slower runoff Q_1 from this box depends on K1 recession constant.	(Seibert, 2005)
SLZ	[mm]	Lower groundwater box (PERC in mm day^{-1} defines the max percolation rate from the upper to the lower groundwater box)	(Seibert, 2005)

1369

1370

1371

1372

1373 *Supplementary Table 1. Initial and final parameter ranges for the multi-criteria model calibration using synthetically derived CRNS S_{NS_SLU} of four SLU units*
1374 *together with observed discharge of the best 50 runs. Parameters Pcorr=1, TT=0, CFMAX=1, CET=1, CFR=0.05, CWH=1 were fixed.*

Initial parameter range				Initial parameter range			
Soil Routine	Lower limit	Upper limit	Final parameter range Median [Min Max]	*Response function*	Lower limit	Upper limit	Final parameter range Median [Min Max]
$BETA_{PastureF}$	1	6	2.5 [1.1-5.5]	$K0_{PastureF}$	0.1	0.8	0.36 [0.13-0.8]
$BETA_{CropI}$	1	6	3.5 [1.3-5.9]	$K0_{CropI}$	0.1	0.8	0.42 [0.11-0.78]
$BETA_{CropP}$	1	6	3.2 [1.1-5.9]	$K0_{CropP}$	0.1	0.8	0.41 [0.14-0.77]
$BETA_{MoorlandP}$	1	4	2.5 [1-3.6]	$K0_{MoorlandP}$	0.1	0.8	0.55 [0.15-0.8]
$FC_{PastureF}$	10	500	318 [50-446]	$K1_{PastureF}$	0.05	0.8	0.63 [0.22-0.79]
FC_{CropI}	10	500	235 [126-477]	$K1_{CropI}$	0.05	0.8	0.59 [0.07-0.8]
FC_{CropP}	10	500	246 [182-327]	$K1_{CropP}$	0.05	0.8	0.67 [0.08-0.79]
$FC_{MoorlandP}$	200	500	318 [210-460]	$K1_{MoorlandP}$	0.1	0.8	0.54 [0.18-0.8]
$LP_{PastureF}$	0.3	1	0.5 [0.3-1]	K2	0.001	0.1	0.054 [0.007-0.098]
LP_{CropI}	0.3	1	0.5 [0.3-0.9]	MAXBAS	1	2.5	1.4 [1-2.3]
LP_{CropP}	0.3	1	0.4 [0.3-1]	$PERC_{PastureF}$	0	4	1.2 [0.2-3.6]
$LP_{MoorlandP}$	0.7	1	0.8 [0.4-1]	$PERC_{CropI}$	0	4	0.5 [0-3.5]
				$PERC_{CropP}$	0	4	1.1 [0-3.7]
				$PERC_{MoorlandP}$	0	4	1.3 [0.1-3.5]
				$UZL_{PastureF}$	0	70	22 [2-67]
				UZL_{CropI}	0	70	40 [0-70]
				UZL_{CropP}	0	70	34 [7-65]
				$UZL_{MoorlandP}$	4	70	43 [7-69]

1375